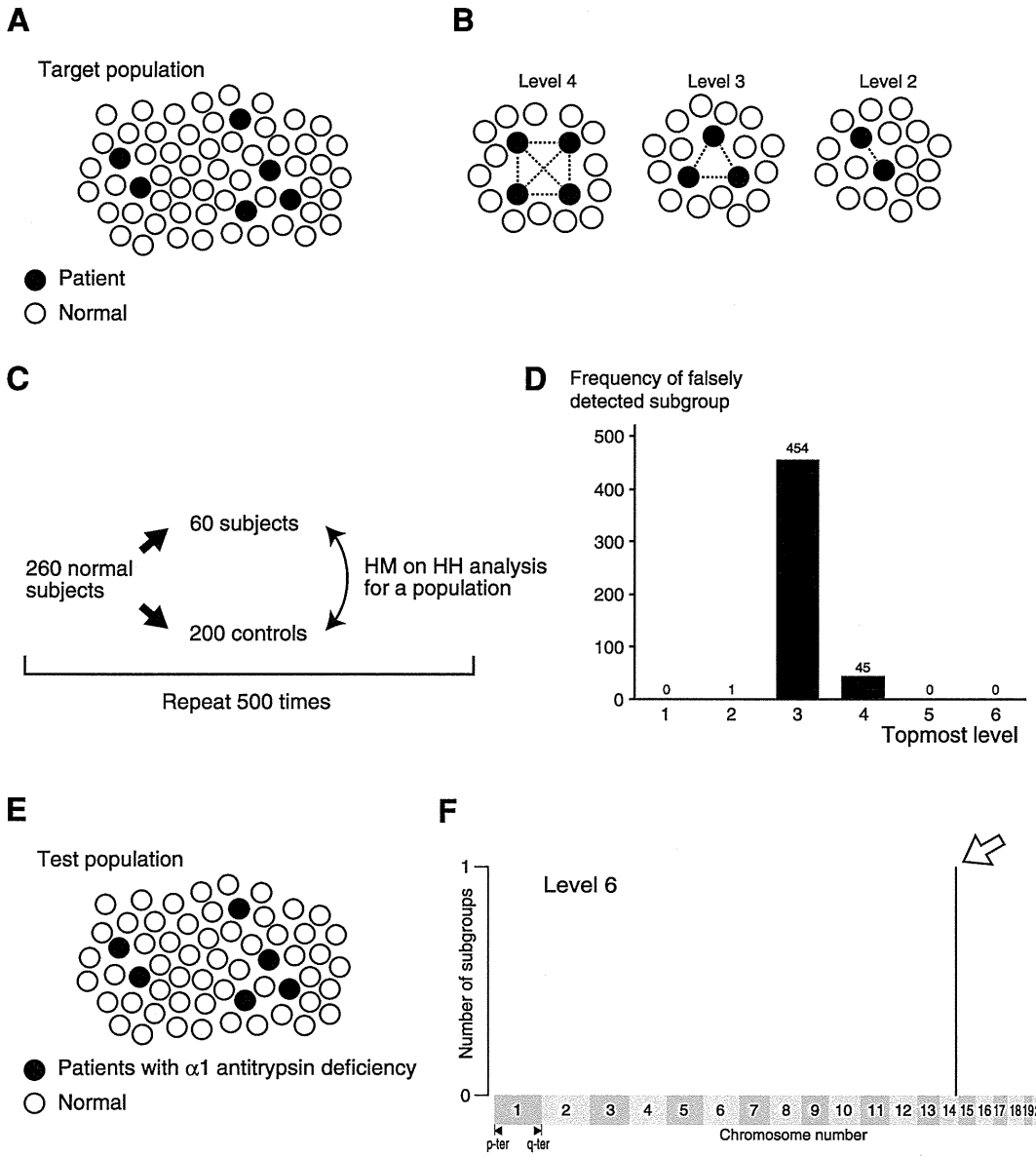

Figure 4. HM on HH analysis of a population. (A) Targets. Targets of HM on HH analysis of a population are populations containing multiple subjects sharing an IBD fragment. (B) Analysis level. At the level *n* analysis, a subgroup of *n* members, each pair of which shares an IBD fragment at the same position on the chromosome, are sought. (C) Scheme of the background determination. (D) Background. A subgroup(s) was falsely detected at level 3, 4, and 5 analyses. (E) A test population. The population is composed of 6 patients with Siiyama-type α1-antitrypsin deficiency (black circles) and 54 normal subjects (white circles). (F) Result. The horizontal position indicates the location on the autosomes, each of which is aligned from the p terminal (left side) to the q terminal (right side). A single subgroup was identified at the level 6 analysis, and the candidate region contained the *SERPINA1* gene. The members of the subgroup, which was the output on the computer console and thus is not shown here, were the 6 patients with Siiyama-type α1-antitrypsin deficiency.
doi:10.1371/journal.pone.0025059.g004

that HM on HH could identify a subpopulation sharing an IBD fragment that accounted for only a small fraction of the population.

The analysis described above assumed that the frequency of the allele containing the disease-causing gene was 0.0 in the general population. However, the disease-causing gene may be a common variant. We investigated the performance of HM on HH analysis when the frequency of the disease-causing gene in the general population was 0.05 or 0.1 (**Figure 5B**). The results indicated that the performance was severely degraded for a frequency of 0.1. HM on HH analysis was considered to work well for a frequency <0.1. Therefore, the HM on HH analysis targets a recessive gene that is the cause of a disease, in which less than 1% of the people in the general population are homozygous for the gene and thus may suffer from the disease somewhere in their lifetime.

Analysis without utilizing HH information

Analyses similar to HM on HH analysis may be performed by stopping the analysis after the HM, IM2, or IM3 steps (**Figure 3A**). When stopping after either the HM or the IM2,

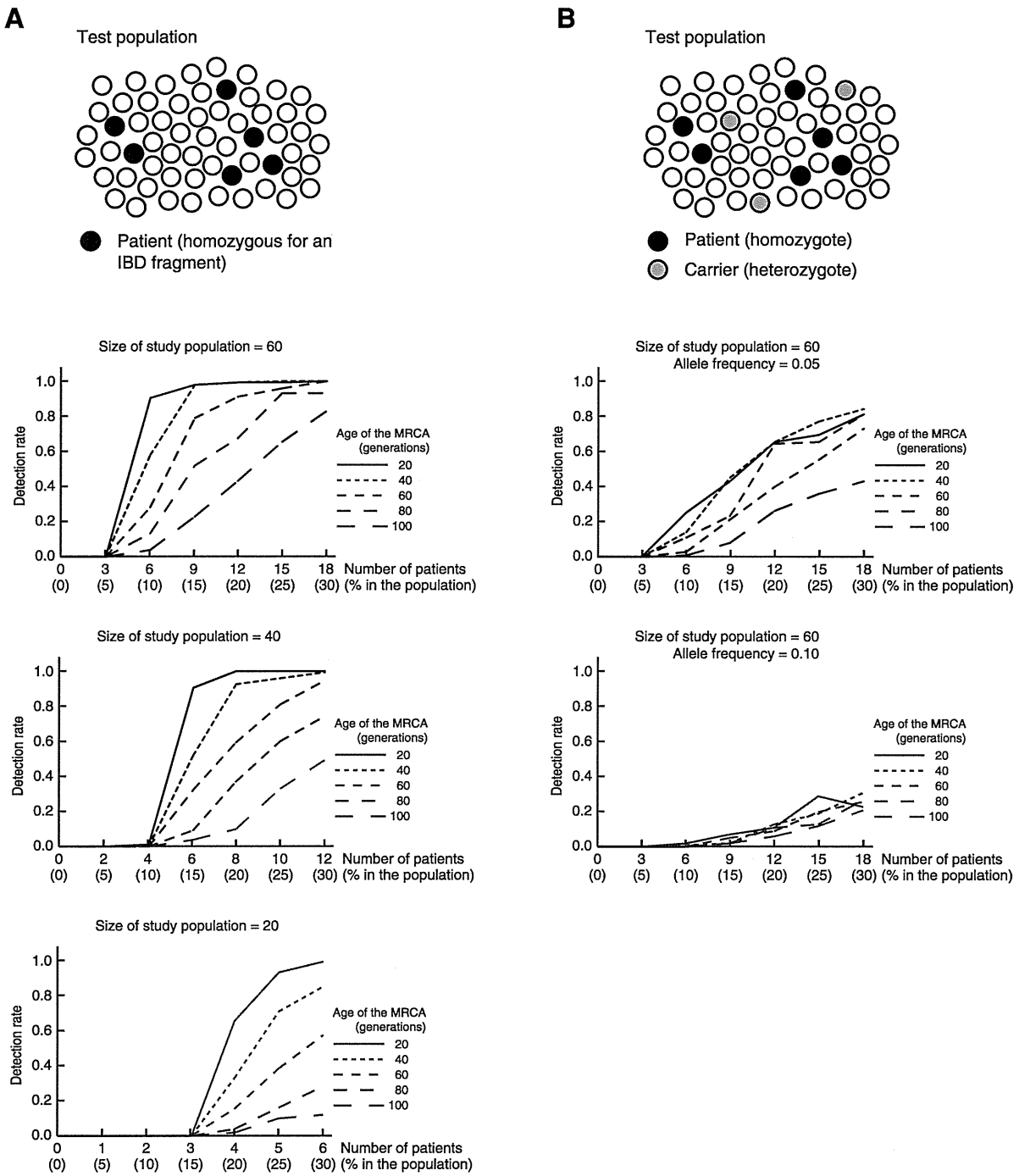

Figure 5. HM on HH analysis of a population performed on populations containing synthetic patients. (A) Scheme of the analysis and Result. The test population is composed of patients homozygous for a gene identical by descent (black circles) and subjects who do not have the gene (white circles). The horizontal line of each graph indicates the number (percentage) of patients homozygous for the gene in the test population. (B) Scheme of the analysis and Result for a gene that is widely shared in the general population. The test population is composed of patients homozygous for a gene identical by descent (black circles), subjects heterozygous for the gene (gray circles), and subjects who do not have the gene (white circles). In the case that the gene was widely shared in the general population (the frequency of the allele of the disease-causing gene was 0.05 and 0.1), the detection rate was decreased.
doi:10.1371/journal.pone.0025059.g005

the program ran out of memory from the explosion in the numbers of subgroups that resulted from a large amount of false positives. When stopping after the IM3 step, the detection rate was much lower than that after the HH analysis, because of a greater amount of false positives (**Figure s3**). These results demonstrated that the small amount of false positives attained by the HH step is important for the performance of HM on HH analysis of a population.

Discussion

In the current report, we demonstrated that HM on HH is able to narrow the candidate region for a disease-causing gene to a very small chromosomal interval either by employing 2 outbred patients sharing an IBD fragment, or by using a small population in which 10%≤ of the patients share an IBD fragment. Haplotype information obtained from the region that flanks the RHSs was the component of the HM on HH analysis that enabled them. By using the HM on HH analysis, genes with a recessive trait are exploited in the very early stage of a project attempting to identify a disease-causing gene.

It has been reported that HM is able to identify a candidate region from as few as 3 inbred patients [5,8]. Although this number is small, the clinical characteristics often do not provide information sufficient for selecting 3 patients who may have an IBD gene. Furthermore, the total length of the candidate regions detected by HM is usually large [8,11], which necessitate an enormous effort for an in-depth search of the regions. HM on HH analysis offers the advantage of being capable of using only 2 patients to obtain a relatively narrow candidate region, typically it is a few centimorgans in length. This may enable novel strategies for identifying disease-causing genes. One such strategy is to collect several patients who are likely to share a fragment IBD, identify the candidate regions by a pairwise comparison, and scrutinize all of these regions by high-throughput sequencing [14].

A small number of founder mutations often largely accounts for the occurrence of a recessive disease or its predisposition. Examples are α1-antitrypsin deficiency and cystic fibrosis in Europeans [15,16], and Gaucher disease and Tay-Sachs disease in Ashkenazi Jews [17]. The cause of the prevalence may be heterozygote advantage, a founder effect, or genetic drift [17,18]. Whatever is the cause, this suggests that the predominance of a limited number of founder mutations is worth taking into consideration in an attempt to search for disease-causing genes with a recessive trait. HM on HH analysis is suitable for pursuing the possibility.

The generational distance of the MRCA has a major effect on the performance of HM on HH analysis. In the analysis of pair of patients, the effect was large (**Figure 3B**). In the analysis of population, the effect was moderate (**Figure 5A**). Use of arrays with a greater number of SNPs will accomplish a better performance (**Figure S1B**). Data obtained using SNP Array 6.0 were investigated in the current study; they were considered suitable for the MRCA with a generational distance ≤60 generations (**Figures 3B and 5A**). Founder populations that settled in recent centuries are amenable to the analysis. These include the French-Canadian population that settled in Quebec in the 17th century [19,20], or the Icelandic population that was founded in the 10th century [21], because the generational distance of the MRCA may be less than 20–60 generations in many diseases.

Isolated populations may also be suitable for this analysis; in such population, a single IBD gene from an MRCA existed in a recent generation may predominate among patients with a specific disease. In many countries, there may be many geographical areas in which MRCAs for a disease-causing gene have a generational distance of 20–60 generations. A small number of patients that HM on HH analysis requires will make the analysis easily performable in small populations from such areas.

Inclusion of the subjects who share the IBD fragment degrades the performance of the analysis. The frequency of the gene in the control should be less than 0.1, i.e., less than 20% of the control subjects may be heterozygous for the gene and less than 1% of the control subjects may be homozygous for the gene. The analysis is not suitable for the common variants for the common diseases that are often the targets of the genome-wide association studies.

The calculation time of the HH on HH analysis is short. The analysis of a pair of patients is completed in a fraction of a second; the analysis for a test population of 60 subjects is completed in 15 seconds. Theoretically, an analysis of a study population of 60 subjects requires an investigation of 1.15×10^{18} subgroups. However, many of the comparison of 2 patients generate a result without any candidate region, and thus eliminate the need for investigating any subgroups containing a given pair. A small amount of false positive of HM on HH analysis enables an exhaustive search for the subgroups.

We used 200 controls in the current study, but it is possible to decrease this number with minimal loss in performance. When the analysis was performed with 100 controls, we found that the performance was only mildly decreased. Moreover, the International HapMap3 project (see International HapMap project Web page) has genotyped and released about 100 or more subjects for each of the 10 ethnic groups, and these data may be used for controls.

The RHS overlap IG-RCHH nest was selected when both the length of the RHS overlap IG and the length of the RCHH between the patients were both at the top. The criteria may be weakened to "top 1%," "top 10%," etc. However, we found that the condition of "at the top" worked best for almost all cases (data not shown). The current criterion is thus considered good for HM on HH analysis.

The RHS cutoff for the Genome-Wide Human SNP Array 6.0 was selected so that the total length of the false-positive RHS was acceptable (1.5 centimorgans per a patient). The equivalent RHS cutoff values for other high-density SNP arrays are 0.75 centimorgans for the Human Omni2.5 BeadChip (Illumina), 1.1 centimorgans for the Human1M-Duo BeadChip (Illumina), and 1.9 centimorgans for the GeneChip Human Mapping 500K Array Set (Affymetrix) [10].

In conclusion, HM on HH analysis used genetic information on both the RHS and the flanking regions, and thus detected the locus for a recessive, disease-causing genes with a very low background from a small number of patients. HM on HH analysis will accelerate the elucidation of the genetic causes of many diseases.

Supporting Information

Figure S1 Errors in the HM. (A) The false positive rate is the ratio of the total length of RHSs that are falsely detected along the entire length of the autosomes. The false negative rate is the ratio of the total length of the autozygous segments (i.e., chromosomal regions in which both chromosomal fragments are IBD) that fail to be detected as RHSs along the total length of the autozygous segments. The false positive rate is dependent on the kind of high-density array and thus is shown for each array. 2.5 M, Human Omni2.5 BeadChip (Illumina); 1 M, Human1M-duo BeadChip (Illuina); SNP6.0: Genome-Wide Human SNP Array 6.0 (Affymetrix); 500K, 500K GeneChips Mapping Array Set (Affymetrix). m: the age of the MRCA. (B) Detection rates for each array. The figure corresponds to **Figure 3B**; this figure summarizes the theoretical calculation, while the result in **Figure 3B** is the result using the actual genotyping data.
(EPS)

Figure S2 Errors in HM on HH for a pair of patients. The data corresponding to those of **Figure 3C** for the MRCAs with a generational distance of 40, 60, 80, and 100 generations.
(EPS)

Figure S3 Result of the analysis stopped after the IM3 step. (A) Background. The background was observed to a higher analysis level than that for the HH analysis (compare with **Figure 4D**). (B) Detection rate. Positive results obtained at a level 7 analysis or higher were considered successful. (C) Detection rate. Positive results obtained at a level 9 analysis or higher were considered successful. Figures (B) and (C) correspond with those shown in **Figure 5A**. In both conditions, the detection rate was lower than those shown in **Figure 5A**.
(EPS)

Acknowledgments

We thank Prof. Tokunaga and Dr. Nao Nishida, Department of Human Genetics, Graduate School of Medicine, University of Tokyo, for providing SNP data for 198 Japanese individuals.

Author Contributions

Conceived and designed the experiments: KH H. Morino HK. Performed the experiments: JS TT H. Miyazawa TS. Analyzed the data: MK YO. Contributed reagents/materials/analysis tools: KS. Wrote the paper: KH MK HK.

References

1. Manolio TA (2010) Genomewide association studies and assessment of the risk of disease. N Engl J Med 363: 166–176.
2. Ott J (1999) Analysis of Human Genetic Linkage. Baltimore, MD: Johns Hopkins University Press.
3. Hardy J, Singleton A (2009) Genomewide association studies and human disease. N Engl J Med 360: 1759–1768.
4. McCarthy MI, Abecasis GR, Cardon LR, Goldstein DB, Little J, et al. (2008) Genome-wide association studies for complex traits: consensus, uncertainty and challenges. Nat Rev Genet 9: 356–369.
5. Lander ES, Botstein D (1987) Homozygosity mapping: a way to map human recessive traits with the DNA of inbred children. Science 236: 1567–1570.
6. Hildebrandt F, Heeringa SF, Ruschendorf F, Attanasio M, Nurnberg G, et al. (2009) A systematic approach to mapping recessive disease genes in individuals from outbred populations. PLoS Genet 5: e1000353.
7. Browning SR, Browning BL (2010) High-resolution detection of identity by descent in unrelated individuals. Am J Hum Genet 86: 526–539.
8. Huqun, Izumi S, Miyazawa H, Ishii K, Uchiyama B, et al. (2007) Mutations in the SLC34A2 gene are associated with pulmonary alveolar microlithiasis. Am J Respir Crit Care Med 175: 263–268.
9. Miyazawa H, Kato M, Awata T, Kohda M, Iwasa H, et al. (2007) Homozygosity haplotype allows a genomewide search for the autosomal segments shared among patients. Am J Hum Genet 80: 1090–1102.
10. Huqun, Fukuyama S, Morino H, Miyazawa H, Tanaka T, et al. (2010) A quantitatively-modeled homozygosity mapping algorithm, qHomozygosityMapping, utilizing whole genome single nucleotide polymorphism genotyping data. BMC Bioinformatics 11 Suppl 7: S5.
11. Maruyama H, Morino H, Ito H, Izumi Y, Kato H, et al. (2010) Mutations of optineurin in amyotrophic lateral sclerosis. Nature 465: 223–226.
12. Seyama K, Nukiwa T, Souma S, Shimizu K, Kira S (1995) Alpha 1-antitrypsin-deficient variant Siiyama (Ser53[TCC] to Phe53[TTC]) is prevalent in Japan. Status of alpha 1-antitrypsin deficiency in Japan. Am J Respir Crit Care Med 152: 2119–2126.
13. Haldane J (1919) The combination of linkage values, and the calculation of distances between the loci of linked factors. J Genet 8: 299–309.
14. Berg JS, Evans JP, Leigh MW, Omran H, Bizon C, et al. (2011) Next generation massively parallel sequencing of targeted exomes to identify genetic mutations in primary ciliary dyskinesia: implications for application to clinical testing. Genet Med 13: 218–229.
15. Janciauskiene SM, Bals R, Koczulla R, Vogelmeier C, Kohnlein T, et al. (2011) The discovery of alpha1-antitrypsin and its role in health and disease. Respir Med 105: 1129–1139.
16. Salvatore D, Buzzetti R, Baldo E, Forneris MP, Lucidi V, et al. (2011) An overview of international literature from cystic fibrosis registries. Part 3. Disease incidence, genotype/phenotype correlation, microbiology, pregnancy, clinical complications, lung transplantation, and miscellanea. J Cystic Fibrosis 10: 71–85.
17. Charrow J (2004) Ashkenazi Jewish genetic disorders. Familial Cancer 3: 201–206.
18. Dean M, Carrington M, O'Brien SJ (2002) Balanced polymorphism selected by genetic versus infectious human disease. Annu Rev Genomics Hum Genet 3: 263–292.
19. Heyer E, Tremblay M (1995) Variability of the genetic contribution of Quebec population founders associated to some deleterious genes. Am J Hum Genet 56: 970–978.
20. Laberge AM, Michaud J, Richter A, Lemyre E, Lambert M, et al. (2005) Population history and its impact on medical genetics in Quebec. Clin Genet 68: 287–301.
21. Williams JT (1993) Origin and population structure of the Icelanders. Hum Biol 65: 167–191.

Biochemical and Biophysical Research Communications 407 (2011) 213–218

Contents lists available at ScienceDirect

Biochemical and Biophysical Research Communications

journal homepage: www.elsevier.com/locate/ybbrc

A novel mutation of ALK2, L196P, found in the most benign case of fibrodysplasia ossificans progressiva activates BMP-specific intracellular signaling equivalent to a typical mutation, R206H

Satoshi Ohte [a,b], Masashi Shin [a], Hiroki Sasanuma [a], Katsumi Yoneyama [a], Masumi Akita [b,c], Kenji Ikebuchi [b,d], Eijiro Jimi [b,e], Yuichi Maruki [b,f], Masaru Matsuoka [b,d], Akira Namba [b,g], Hiroshi Tomoda [b,h], Yasushi Okazaki [b,i], Akira Ohtake [b,j], Hiromi Oda [b,k], Ichiro Owan [b,l], Tetsuya Yoda [b,m], Hirokazu Furuya [n], Jyunji Kamizono [o,p], Hiroshi Kitoh [o,q], Yasuharu Nakashima [o,r], Takafumi Susami [o,s], Nobuhiko Haga [o,t], Tetsuo Komori [b,u], Takenobu Katagiri [a,b,o,*]

[a] Division of Pathophysiology, Research Center for Genomic Medicine, Saitama Medical University, 1397-1 Yamane, Hidaka-shi, Saitama 350-1241, Japan
[b] Project of Clinical and Basic Research for FOP at Saitama Medical University, Japan
[c] Division of Morphological Science, Biomedical Research Center, Saitama Medical University, 38 Moro Hongo, Moroyama-machi, Iruma-gun, Saitama 350-0495, Japan
[d] Division of Laboratory Medicine, Saitama Medical University, 38 Moro Hongo, Moroyama-machi, Iruma-gun, Saitama 350-0495, Japan
[e] Division of Molecular Signaling and Biochemistry, Department of Biosciences, Kyushu Dental Collage, 2-6-1Manazuru, Kokurakita-ku, Kitakyushu-shi, Fukuoka 803-8580, Japan
[f] Department of Neurology, Saitama Neuropsychiatric Institute, 6-11-1 Honchohigashi, Chuo-ku, Saitama-shi, Saitama 338-8577, Japan
[g] Division of Obstetrics and Gynecology, Saitama Medical University, 38 Moro Hongo, Moroyama-machi, Iruma-gun, Saitama 350-0495, Japan
[h] Graduate School of Pharmaceutical Sciences, Kitasato University, 5-9-1 Shirokane, Minato-ku, Tokyo 108-0023, Japan
[i] Division of Functional Genomics & Systems Medicine, Research Center for Genomic Medicine, Saitama Medical University, 1397-1 Yamane, Hidaka-shi, Saitama 350-1241, Japan
[j] Division of Pediatrics, Saitama Medical University, 38 Moro Hongo, Moroyama-machi, Iruma-gun, Saitama 350-0495, Japan
[k] Division of Orthopedic Surgery, Saitama Medical University, 38 Moro Hongo, Moroyama-machi, Iruma-gun, Saitama 350-0495, Japan
[l] Department of Orthopedic Surgery, University of Ryukyus Faculty of Medicine, 207 Uehara, Nishihara-cho, Okinawa 903-0215, Japan
[m] Division of Oral and Maxillofacial Surgery, Saitama Medical University, 38 Moro Hongo, Moroyama-machi, Iruma-gun, Saitama 350-0495, Japan
[n] Department of Neurology, Neuro-Muscular center, National Omuta Hospital, Tachibana 1044-1, Omuta, Fukuoka 837-0911, Japan
[o] The Research Committee on Fibrodysplasia Ossificans Progressiva of the Ministry of Health, Labour and Welfare, Japan
[p] Kitakyushu City Yahata Hospital Pediatric Emergency Department, 4-18-1 Nishihon-machi, Yahatahigashi-ku, Kitakyushu-shi, Fukuoka 805-0061, Japan
[q] Department of Orthopedic Surgery, Graduate School of Medicine, Nagoya University, 65 Tsurumai-cho, Showa-ku, Nagoya 466-8550, Japan
[r] Department of Orthopaedic Surgery, Faculty of Medicine, Kyushu University, 3-1-1, Maidashi, Higashi-ku, Fukuoka-shi, Fukuoka 812-8582, Japan
[s] Department of Oral-Maxillofacial Surgery, Dentistry and Orthodontics, The University of Tokyo Hospital, 7-3-1 Hongo, Bunkyo-ku, Tokyo 113-8655, Japan
[t] Department of Rehabilitation Medicine, The University of Tokyo Hospital, 7-3-1 Hongo, Bunkyo-ku, Tokyo 113-8655, Japan
[u] Department of Neurology, National Hakone Hospital, 412 Kazamatsuri, Odawara-shi, Kanagawa 250-0032, Japan

ARTICLE INFO

Article history:
Received 28 February 2011
Available online 4 March 2011

Keywords:
FOP
ALK2
BMP
Smad
Muscle
Signaling

ABSTRACT

Fibrodysplasia ossificans progressiva (FOP) is a rare autosomal dominant congenital disorder characterized by progressive heterotopic ossification in muscle tissues. Constitutively activated mutants of a bone morphogenetic protein (BMP) receptor, ALK2, have been identified in patients with FOP. Recently, a novel ALK2 mutation, L196P, was found in the most benign case of FOP reported thus far. In the present study, we examined the biological activities of ALK2(L196P) *in vitro*. Over-expression of ALK2(L196P) induced BMP-specific activities, including the suppression of myogenesis, the induction of alkaline phosphatase activity, increased BMP-specific luciferase reporter activity, and increased phosphorylation of Smad1/5 but not Erk1/2 or p38. The activities of ALK2(L196P) were higher than those of ALK2(G356D), another mutant ALK2 allele found in patients with FOP and were equivalent to those of ALK2(R206H), a typical mutation found in patients with FOP. ALK2(L196P) was equally or more resistant to inhibitors in comparison to ALK2(R206H). These findings suggest that ALK2(L196P) is an activated BMP receptor equivalent to ALK2(R206H) and that ALK2(L196P) activity may be suppressed *in vivo* by a novel molecular mechanism in patients with this mutation.

Abbreviations: ALK2, activin receptor-like kinase 2; ALP, alkaline phosphatase; BMP, bone morphogenetic protein; FOP, fibrodysplasia ossificans progressiva; MAPK, mitogen-activated protein kinase; TGF-β, transforming growth factor-β.

* Corresponding author at: Division of Pathophysiology, Research Center for Genomic Medicine, Saitama Medical University, 1397-1 Yamane, Hidaka-shi, Saitama 350-1241, Japan. Fax: +81 42 984 4651.
E-mail address: katagiri@saitama-med.ac.jp (T. Katagiri).

0006-291X/$ - see front matter © 2011 Elsevier Inc. All rights reserved.
doi:10.1016/j.bbrc.2011.03.001

1. Introduction

Fibrodysplasia ossificans progressiva (FOP; OMIM135100) is a rare hereditary disorder that is characterized by postnatal progressive heterotopic ossification in soft tissues, especially skeletal muscle [1–3]. The heterotopic ossification in FOP starts during childhood, and most patients with FOP shows congenital malformation of the great toes at birth [1–4]. In FOP, acute heterotopic ossification is induced by muscle injury, such as accidental trauma or surgical operations. There is no effective treatment for preventing the heterotopic ossification associated with FOP.

The ACVR1 gene on chromosome 2q23-24 has been identified as the gene responsible for both familial and sporadic cases of FOP [5]. ACVR1 encodes the ALK2 protein, which is one of the signaling receptors for bone morphogenetic proteins (BMPs) [3,6,7]. BMPs induce heterotopic bone formation in skeletal muscle *in vivo* and initiate the differentiation pathway through which myoblasts convert to osteoblastic cells *in vitro* [8,9]. ALK2 is a transmembrane serine/threonine kinase receptor that activates intracellular signaling pathways via Smad1/5, Erk1/2, and p38 in response to BMP binding [3,6,7]. A substitution mutation in ALK2 from arginine to histidine at codon 206 (R206H) has been found in patients with FOP [5]. This ALK2 mutant activates BMP-specific intracellular signaling without binding to ligands, similar to ALK2(Q207), which is an experimentally identified active ALK2 variant [10]. Thus, FOP was the first disease identified as a gain-of-function mutation involving the signaling receptors for BMPs and related ligands.

Several mutations at different positions within ALK2 have been identified in atypical FOP patients who show variations in clinical features, such as the progression of heterotopic ossification and/or finger development [11,12]. Among these mutations, the G356D mutation was found in one patient who had severe toe malformation and mild heterotopic bone formation in muscle in comparison to typical patients with FOP, who have an ALK2(R206H) allele [11]. We reported that ALK2(G356D) was also an activated BMP receptor but that it was weaker than ALK2(R206H) *in vitro* [13]. It has been suggested that quantitative differences in the biological activities of ALK2 mutants may cause the differences in clinical features in patients with FOP [13]. However, the molecular mechanisms of the regulation of these mutant ALK2 receptors are still unclear.

Recently, a novel mutation in ALK2, L196P, was found in the most benign FOP variant case reported in the literature thus far [14]. In contrast to other patients with FOP, this patient had neither great toe malformations at birth nor heterotopic ossification in skeletal muscle until a motorcycle accident at age 21 [14]. To examine the molecular mechanisms of this mild phenotype, we compared the biological activities of ALK2(L196P) with other ALK2 mutants *in vitro*. Unexpectedly, we found that ALK2(L196P) showed almost equivalent activities compared to ALK2(R206H), and it was less sensitive than ALK2(R206H) to protein inhibitors, such as Smad6 and FKBP12. These findings suggest that the activity of L196P might be masked by a novel *in vivo* mechanism in patients with this mutation. Such an inhibitory mechanism may aid in the establishment of a new treatment strategy to prevent heterotopic ossification in FOP.

2. Material and methods

2.1. Plasmids and cell cultures

The V5-tagged human ALK2 expression vector was used [12,13]. ALK2(L196P) was obtained via a standard PCR technique using the primers CAGGAAGTGGCTCTGGTCCTCCTTTTCTGGTAC and GTACCAGAAAAGGAGGACCAGAGCCACTTCCTG, and its DNA sequence was confirmed using an ABI3500 Genetic Analyzer (Applied Biosystems, Foster City, CA). A new version of the BMP-specific IdWT4F-luc reporter was constructed by transferring four copies of the BMP-responsive element from the original IdWT4F-luc in pGL3-Promoter [15] to pGL4.26 (Promega, Madison, WI). Other ALK2 mutants, CAGA-luc, and FLAG-tagged Smad1, Smad5, Smad6, Smad7, Smad8, FKBP12, and MyoD have been described previously [12,13,15,16]. Murine C2C12 myoblasts and C3H10T1/2 clone 8 fibroblasts were maintained in Dulbecco's modified Eagle's medium containing 15% fetal bovine serum [9,17].

2.2. Luciferase reporter assay

The luciferase reporter assay was performed using IdWT4F-luc or CAGA-luc with phRL-SV40 for normalization of transfection efficiency [15,18]. C2C12 cells were inoculated at 1×10^4 cells/well in a 96-well plate one day prior to the assay. The cells were transfected with 200 ng of plasmid DNA using Lipofectamine 2000 (Invitrogen, Carlsbad, CA) according to the manufacturer's instructions. The firefly and renilla luciferase activities were determined using the Dual-Glo Luciferase Assay Kit (Promega).

2.3. Alkaline phosphatase activity

Alkaline phosphatase (ALP) activity was determined as a typical marker of osteoblastic differentiation [9,19]. C2C12 cells were incubated in a substrate solution (0.1 M diethanolamine, 1 mM $MgCl_2$, and 1 mg/ml p-nitrophenylphosphate) for 30 min at room temperature. Reactions were terminated by adding 3 M NaOH, and the absorbance was measured at 405 nm [19].

2.4. Immunostaining

Myogenesis was induced in C3H10T1/2 cells and tested using immunohistochemical staining of myosin heavy chain (MHC) on day 3 using an antibody (clone MF-20, Developmental Studies Hybridoma Bank, Iowa City, IA) and a Histofine SimpleStain Kit (Nichirei, Tokyo, Japan) [9,17]. The cellular localization of phospho-Smad1/5 and V5-tagged ALK2 in C2C12 cells was determined by immunohistochemical staining using an anti-phospho-Smad1/5 rabbit monoclonal antibody (clone 41D10, Cell Signaling, Beverly, MA) and an anti-V5 mouse monoclonal antibody (clone V5005, Nacalai Tesque, Kyoto, Japan), respectively [10,13,16]. Target proteins were visualized using an Alexa Fluor 488- or Alexa Fluor 594-conjugated secondary antibody (Invitrogen).

2.5. Western blot analysis

C2C12 cells were lysed in TNE buffer and subjected to western blotting as described previously [10,13,16]. The following antibodies were used: anti-phospho-Smad1/5/8 rabbit polyclonal (Cell Signaling), anti-phospho-p38 rabbit monoclonal (clone 3D7, Cell Signaling), anti-phospho-Erk1/2 rabbit monoclonal (clone D13.14.4E, Cell Signaling), anti-FLAG mouse monoclonal (clone M2, Sigma, St. Louis, MO), anti-V5 mouse monoclonal and anti-α-tubulin rabbit polyclonal (Cell Signaling). The target proteins were detected using a horseradish peroxidase-conjugated anti-mouse or anti-rabbit IgG antibody (GE Healthcare, Buckinghamshire, England) and a Chemi-Lumi One Super (Nacalai Tesque).

2.6. Statistical analysis

Comparisons were made using Student's *t*-test. Results were expressed as the mean ± SD ($n = 3$). Statistical significance was indicated as $^*p < 0.05$ and $^{**}p < 0.01$.

3. Results

3.1. ALK2(L196P) is an activated BMP receptor equivalent to ALK2(R206H)

First, we compared the biological activities of ALK2(L196P) with other ALK2 mutants found in FOP: R206H, G356D, and an experimentally established active mutant, Q207D. In the absence of BMPs, the BMP-specific luciferase reporter IdWT4F-luc was activated 30-fold, 37-fold, 13-fold and 46-fold by the ALK2 mutants L196P, R206H, G356D and Q207D, respectively (Fig. 1A). In contrast to IdWT4F-luc, a TGF-β/activin-specific reporter, CAGA-luc, was not activated by any ALK2 receptor examined (Fig. 1B). The *in vitro* suppression of myogenesis was examined as another marker of BMP activity. The numbers of myosin heavy chain-expressing myogenic cells were decreased in response to the over-expression of ALK2 mutants but not wild-type ALK2 (Fig. 1C). Treatment of parental C2C12 cells with 50 ng/ml of BMP-6 increased alkaline phosphatase activity; which was further increased in response to the over-expression of ALK2 mutant L196P, R206H, G356D, and Q207D alleles (Fig. 1D). In the absence of BMP-6, weak ALP activity was induced only in response to ALK2(Q207D). These findings indicate that ALK2(L196P) is an activated BMP receptor equivalent to ALK2(R206H).

3.2. ALK2(L196P) activates osteoblastic differentiation via the BMP-specific Smad-dependent pathway

We next examined intracellular signaling pathways involved in the BMP activities induced by ALK2(L196P). Over-expression of ALK2(L196P), ALK2(R206H) or ALK2(Q207D) induced phosphorylation of endogenous Smad1/5 in the nuclei of C2C12 cells (Fig. 2A). These mutant ALK2 proteins induced phosphorylation of exogenous FLAG-Smad1 in the following order: Q207D ≫ L196P = R206H ≫ G356D. Neither phospho-Erk1/2 nor phospho-p38 was induced by any mutant ALK2 receptor (Fig. 2B). Co-transfection of one of the mutant ALK2 receptors into C2C12 cells increased ALP activity in cooperation with not only FLAG-Smad1 but also FLAG-Smad5 and FLAG-Smad8 (Fig. 2C). As reported previously, Smad8 showed the lowest activity [10]. The order of ALP activity induction was similar to that of the capacity to phosphorylate exogenous FLAG-Smad1, suggesting that the BMP-specific Smad pathway mediates ALK2-induced osteoblastic differentiation. This result was confirmed by the suppression of ALP activity induced by ALK2 and FLAG-Smad1 by LDN-193189, a specific chemical inhibitor of the phosphorylation of Smad1/5/8 by BMP receptors (Fig. 2D).

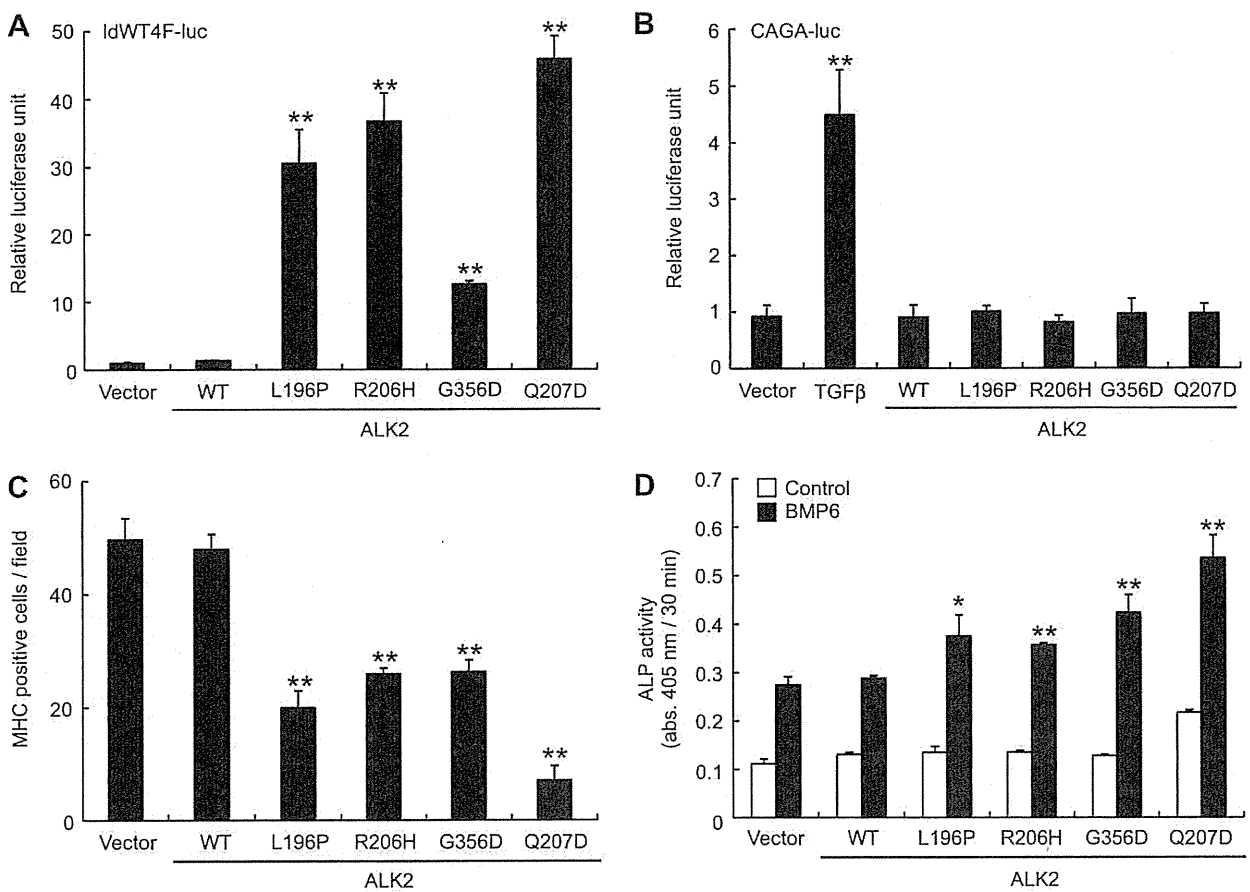

Fig. 1. ALK2(L196P) is an activated BMP receptor. (A and B) BMP-specific and TGF-β-specific luciferase assay. IdWT4F-luc (A) or CAGA-luc (B) was co-transfected with wild-type (WT) or one mutant allele of ALK2 (L196P, R206H, G356D or Q207D) into C2C12 cells. (C) Suppression of myogenesis by ALK2. The numbers of myosin heavy chain (MHC)-positive cells were counted on day 3 in C3H10T1/2 cell cultures transfected with MyoD and one of the ALK2 plasmids as indicated. (D) ALP activity induced by the cooperation of ALK2 and BMP-6. C2C12 cells were transfected with one of the ALK2 plasmids as indicated and cultured for three days with or without 50 ng/ml of BMP-6. Results are presented as the means ± SD ($n = 3$). $^{*}P < 0.05$ and $^{**}P < 0.01$ in comparison with cells transfected with an empty vector in each group.

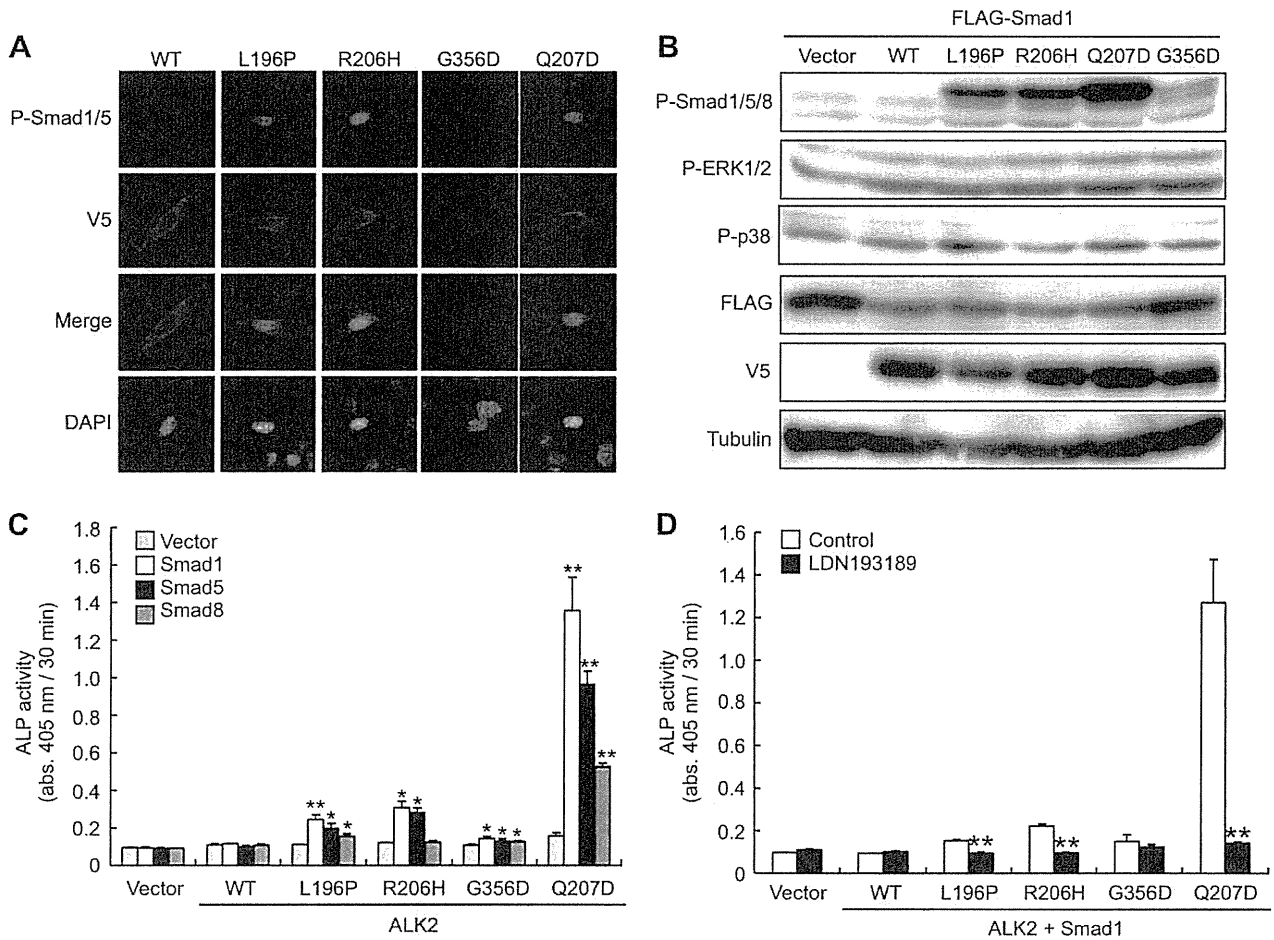

Fig. 2. ALK2(L196P) induces the Smad1/5-dependent pathway but not the non-Smad- or the Smad2/3-dependent pathways. (A) Immunohistochemical analysis of endogenous phospho-Smad1/5. C2C12 cells transfected with one of the V5-tagged ALK2 plasmids indicated were double-stained with anti-phospho-Smad1/5 (green) and anti-V5 (red) antibodies. (B) Western blot analysis of intracellular signaling pathways activated by ALK2 receptors. C2C12 cells were co-transfected with FLAG-tagged Smad1 and one of the V5-tagged ALK2 constructs. Cell lysates were immunoblotted with antibodies against phospho-Smad1/5/8, phospho-Erk1/2, phospho-p38, FLAG-tag, V5-tag and a-tubulin. (C) ALP activity induced by the cooperation of ALK2 and Smad1/5/8. C2C12 cells were co-transfected with one of the ALK2 plasmids as indicated and FLAG-tagged Smad1, Smad5 or Smad8 and cultured for three days in the absence of BMPs. The results are presented as the means ± SD ($n = 3$). $^{*}P < 0.05$ and $^{**}P < 0.01$ in comparison with cells transfected with an empty vector in each group. (D) Activation of the BMP-regulated Smads is involved in osteoblastic differentiation induced by ALK2. C2C12 cells were co-transfected with one of the ALK2 plasmids as indicated and FLAG-tagged Smad1 and cultured for three days with or without 100 nM LDN-193189. Results are presented as the means ± SD ($n = 3$). $^{*}P < 0.05$ and $^{**}P < 0.01$ compared with controls.

3.3. *Effects of protein and chemical inhibitors on mutant ALK2 activities*

To examine the molecular mechanisms of the mild phenotypes of the FOP patient with activated ALK2(L196P), we examined the sensitivity of ALK2(L196P) to protein inhibitors and compared it to that of ALK2(R206H). Co-expression of Smad6, Smad7 or FKBP-12 dose-dependently suppressed the IdWT4F-luc activity induced by ALK2(L196P) or ALK2(R206H). The IC_{50} values of inhibitors against ALK2(L196P) were higher than those of ALK2(R206H) (Fig. 3A–C). The IdWT4F-luc induced by ALK2(L196P) or ALK2(R206H) was dose-dependently suppressed by the chemical inhibitor LDN-193189 (Fig. 3D). However, ALK2(L196P) was slightly more resistant than ALK2(R206H) to LDN-193189 (Fig. 3D).

4. Discussion

In the present study, we examined the molecular mechanisms of a novel ALK2 mutation, ALK2(L196P), found in the most benign case of FOP reported in the literature thus far [14]. We speculated that ALK2(L196P) was a more weakly activating mutation than other ALK2 mutations found in typical and atypical FOP patients because the patient with this mutation did not have toe malformations at birth and had delayed induction of heterotopic ossification in skeletal muscle [14]. Unexpectedly, however, ALK2(L196P) showed higher activity than ALK2(G356D) and equivalent activity to ALK2(R206H), a typical FOP variant mutation, suggesting that ALK2(L196P) activity may be suppressed by a novel mechanism in this patient. To examine this possibility, we compared the sensitivity of ALK2(L196P) receptors to different protein inhibitors, including FKBP12, that have been shown to be involved in the activation of ALK2 in FOP [20]. However, ALK2(L196P) was more resistant rather than more sensitive to Smad6 and FKBP12 than was ALK2(R206H). Thus, a novel inhibitor may be involved in the regulation of ALK2(L196P) *in vivo*. It is possible that such an inhibitory mechanism of ALK2 activity will aid in the establishment of novel therapeutic strategies for FOP patients with other ALK2 mutations. Further studies will be required to examine this possibility.

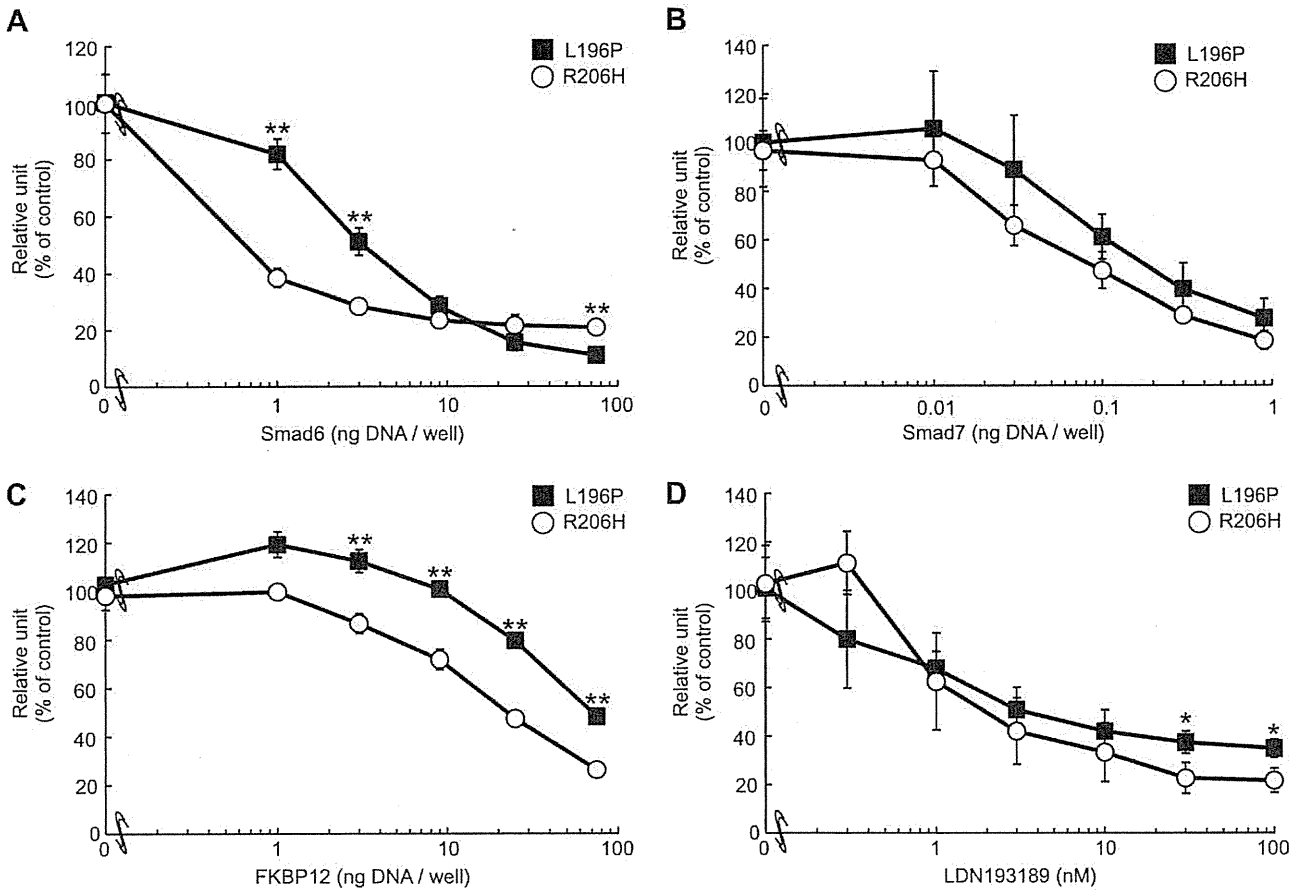

Fig. 3. Effects of protein and chemical inhibitors on ALK2(L196P) and ALK2(R206H). The BMP-specific IdWT4F-luc was activated by the transfection of C2C12 cells with ALK2(L196P) (closed squares) or ALK2(R206H) (open circles). The effects of inhibitors (Smad6 (A), Smad7 (B), FKBP12 (C) and LDN-193189 (D)) on ALK2(L196P) and ALK2(R206H) were determined using IdWT4F-luc in C2C12 cells. The cells were co-transfected with IdWT4F-luc, one of the ALK2 plasmids as indicated and varying amounts of Smad6 (A), Smad7 (B), or FKBP12 (C). The cells were cultured in the presence of varying concentrations of LDN-193189 (D). Total amounts of transfected DNA were adjusted equally with an empty vector. Luciferase activity was determined on day 1. Results are presented as the means (% of control) ± SD ($n = 3$). $^{*}P < 0.05$ and $^{**}P < 0.01$ in comparison with transfection with L196P and R206H.

The induction of the osteoblastic differentiation of myoblasts by ALK2 seems to be dependent on its kinase activity, which phosphorylates Smad1/5 at its carboxyl termini [13]. The degree to which ALP activity was induced by the co-transfection of ALK2 and Smad1 was the same as the degree of the phosphorylation levels of Smads by ALK2 mutants. Moreover, ALK2(L196P) and other mutant ALK2 variants did not activate the non-Smad MAPK or the TGF-b-specific Smad pathways. Recently, we showed that a constitutively activated Smad1, in which the carboxyl phosphorylation sites of BMP receptors were substituted with different acidic amino acids, induced osteoblastic differentiation of C2C12 myoblasts in the absence of BMPs [16]. Taken together, these findings suggest that the phosphorylation of Smad1/5 by mutant ALK2 receptors is one of the most critical targets to prevent heterotopic ossification in FOP. Indeed, the osteoblastic differentiation of C2C12 cells induced by ALK2 mutants was blocked by the chemical inhibitors dorsomorphin and LDN-193189 [10,13]. LDN-193189 has been shown to suppress heterotopic ossification induced by ALK2(Q207D) *in vivo* [21].

In conclusion, a mutant ALK2, ALK2(L196P), found in the most benign case of FOP reported thus far is an activated BMP receptor in the absence of BMPs, and it has equivalent *in vitro* activity to a typical mutation, ALK2(R206H). The *in vivo* biological activity of ALK2(L196P) may be masked by a novel, as yet undiscovered molecular mechanism in this patient.

Acknowledgments

We thank Dr. Kohei Miyazono, Department of Molecular Pathology, Graduate School of Medicine, The University of Tokyo and members of the Division of Pathophysiology, Research Center for Genomic Medicine, Saitama Medical University, for their valuable comments. We are grateful to Dr. J. A. Langer for kindly providing pcDEF3. This work was supported in part by Health and Labour Sciences Research Grants for Research on Measures for Intractable Research from the Ministry of Health, Labour and Welfare of Japan, grants-in-aid from The Ministry of Education, Culture, Sports, Science, and Technology of Japan, a grant-in-aid from The Takeda Science Foundation, a grant-in-aid from The Suzuken memorial foundation, and a grant-in-aid for the "Support Project of Strategic Research Center in Private Universities" from The Ministry of Education, Culture, Sports, Science and Technology (MEXT) to Saitama Medical University Research Center for Genomic Medicine.

References

[1] F.S. Kaplan, Q. Shen, V. Lounev, P. Seemann, J. Groppe, T. Katagiri, R.J. Pignolo, E.M. Shore, Skeletal metamorphosis in fibrodysplasia ossificans progressiva (FOP), J. Bone Miner. Metab. 26 (2008) 521–530.

[2] F.S. Kaplan, M. Le Merrer, D.L. Glaser, R.J. Pignolo, R.E. Goldsby, J.A. Kitterman, J. Groppe, E.M. Shore, Fibrodysplasia ossificans progressiva, Best Pract. Res. Clin. Rheumatol. 22 (2008) 191–205.

[3] T. Katagiri, Heterotopic bone formation induced by bone morphogenetic protein signaling: fibrodysplasia ossificans progressiva, J. Oral Biosci. 52 (2010) 33–41.
[4] K. Mishima, H. Kitoh, T. Katagiri, H. Kaneko and N. Ishiguro, Early clinical and radiological characteristics in fibrodysplasia ossificans progressiva. A report of two cases, J. Bone Joint Surg. (2011), in press.
[5] E.M. Shore, M. Xu, G.J. Feldman, D.A. Fenstermacher, T.J. Cho, I.H. Choi, J.M. Connor, P. Delai, D.L. Glaser, M. LeMerrer, R. Morhart, J.G. Rogers, R. Smith, J.T. Triffitt, J.A. Urtizberea, M. Zasloff, M.A. Brown, F.S. Kaplan, A recurrent mutation in the BMP type I receptor ACVR1 causes inherited and sporadic fibrodysplasia ossificans progressiva, Nat. Genet. 38 (2006) 525–527.
[6] K. Miyazono, S. Maeda, T. Imamura, BMP receptor signaling: transcriptional targets, regulation of signals, and signaling cross-talk, Cytokine Growth Factor Rev. 16 (2005) 251–263.
[7] T. Katagiri Suda, T.K. Miyazono, The bone morphogenetic proteins, In The TGF-b Family, in: R. Derynck, K. Miyazono (Eds.), Cold Spring Harbor Press, New York, 2008, pp. 121–149.
[8] M.R. Urist, Bone: formation by autoinduction, Science 150 (1965) 893–899.
[9] T. Katagiri, A. Yamaguchi, M. Komaki, E. Abe, N. Takahashi, T. Ikeda, V. Rosen, J.M. Wozney, A. Fujisawa-Sehara, T. Suda, Bone morphogenetic protein-2 converts the differentiation pathway of C2C12 myoblasts into the osteoblast lineage, J. Cell Biol. 127 (1994) 1755–1766.
[10] T. Fukuda, M. Kohda, K. Kanomata, J. Nojima, A. Nakamura, J. Kamizono, Y. Noguchi, K. Iwakiri, T. Kondo, J. Kurose, K.I. Endo, T. Awakura, J. Fukushi, Y. Nakashima, T. Chiyonobu, A. Kawara, Y. Nishida, I. Wada, M. Akita, T. Komori, K. Nakayama, A. Nanba, Y. Maruki, T. Yoda, H. Tomoda, P.B. Yu, E.M. Shore, F.S. Kaplan, K. Miyazono, M. Matsuoka, K. Ikebuchi, O. Akira, O. Hiromi, J. Eijiro, O. Ichiro, O. Yasushi, K. Takenobu, Constitutively activated ALK2 and increased smad1/5 cooperatively induce BMP signaling in fibrodysplasia ossificans progressiva, J. Biol. Chem. 284 (2009) 7149–7156.
[11] H. Furuya, K. Ikezoe, L. Wang, Y. Ohyagi, K. Motomura, N. Fujii, J. Kira, Y. Fukumaki, A unique case of fibrodysplasia ossificans progressiva with an ACVR1 mutation, G356D, other than the common mutation (R206H), Am. J. Med. Genet. A 146A (2008) 459–463.
[12] F.S. Kaplan, M. Xu, P. Seemann, J.M. Connor, D.L. Glaser, L. Carroll, P. Delai, E. Fastnacht-Urban, S.J. Forman, G. Gillessen-Kaesbach, J. Hoover-Fong, B. Koster, R.M. Pauli, W. Reardon, S.A. Zaidi, M. Zasloff, R. Morhart, S. Mundlos, J. Groppe, E.M. Shore, Classic and atypical fibrodysplasia ossificans progressiva (FOP) phenotypes are caused by mutations in the bone morphogenetic protein (BMP) type I receptor ACVR1, Hum. Mutat. 30 (2009) 379–390.
[13] T. Fukuda, K. Kanomata, J. Nojima, S. Kokabu, M. Akita, K. Ikebuchi, E. Jimi, T. Komori, Y. Maruki, M. Matsuoka, K. Miyazono, K. Nakayama, A. Nanba, H. Tomoda, Y. Okazaki, A. Ohtake, H. Oda, I. Owan, T. Yoda, N. Haga, H. Furuya, T. Katagiri, A unique mutation of ALK2, G356D, found in a patient with fibrodysplasia ossificans progressiva is a moderately activated BMP type I receptor, Biochem. Biophys. Res. Commun. 377 (2008) 905–909.
[14] C.L. Gregson, P. Hollingworth, M. Williams, K.A. Petrie, A.N. Bullock, M.A. Brown, J.H. Tobias, J.T. Triffitt, A novel ACVR1 mutation in the glycine/serine-rich domain found in the most benign case of a fibrodysplasia ossificans progressiva variant reported to date, Bone 48 (2011) 654–658.
[15] T. Katagiri, M. Imada, T. Yanai, T. Suda, N. Takahashi, R. Kamijo, Identification of a BMP-responsive element in Id1, the gene for inhibition of myogenesis, Genes Cells 7 (2002) 949–960.
[16] J. Nojima, K. Kanomata, Y. Takada, T. Fukuda, S. Kokabu, S. Ohte, T. Takada, T. Tsukui, T.S. Yamamoto, H. Sasanuma, K. Yoneyama, N. Ueno, Y. Okazaki, R. Kamijo, T. Yoda, T. Katagiri, Dual roles of smad proteins in the conversion from myoblasts to osteoblastic cells by bone morphogenetic proteins, J. Biol. Chem. 285 (2010) 15577–15586.
[17] T. Katagiri, S. Akiyama, M. Namiki, M. Komaki, A. Yamaguchi, V. Rosen, J.M. Wozney, A. Fujisawa-Sehara, T. Suda, Bone morphogenetic protein-2 inhibits terminal differentiation of myogenic cells by suppressing the transcriptional activity of MyoD and myogenin, Exp. Cell Res. 230 (1997) 342–351.
[18] H. Suzuki, K. Yagi, M. Kondo, M. Kato, K. Miyazono, K. Miyazawa, c-Ski inhibits the TGF-beta signaling pathway through stabilization of inactive Smad complexes on Smad-binding elements, Oncogene 23 (2004) 5068–5076.
[19] K. Kodaira, M. Imada, M. Goto, A. Tomoyasu, T. Fukuda, R. Kamijo, T. Suda, K. Higashio, T. Katagiri, Purification and identification of a BMP-like factor from bovine serum, Biochem. Biophys. Res. Commun. 345 (2006) 1224–1231.
[20] Q. Shen, S.C. Little, M. Xu, J. Haupt, C. Ast, T. Katagiri, S. Mundlos, P. Seemann, F.S. Kaplan, M.C. Mullins, E.M. Shore, The fibrodysplasia ossificans progressiva R206H ACVR1 mutation activates BMP-independent chondrogenesis and zebrafish embryo ventralization, J. Clin. Invest. 119 (2009) 3462–3472.
[21] P.B. Yu, D.Y. Deng, C.S. Lai, C.C. Hong, G.D. Cuny, M.L. Bouxsein, D.W. Hong, P.M. McManus, T. Katagiri, C. Sachidanandan, N. Kamiya, T. Fukuda, Y. Mishina, R.T. Peterson, K.D. Bloch, BMP type I receptor inhibition reduces heterotopic ossification, Nat. Med. 14 (2008) 1363–1369.

Cell Stem Cell
Article

Indefinite Self-Renewal of ESCs through Myc/Max Transcriptional Complex-Independent Mechanisms

Tomoaki Hishida,[1,4] Yuriko Nozaki,[1,4] Yutaka Nakachi,[2] Yosuke Mizuno,[2] Yasushi Okazaki,[2,4] Masatsugu Ema,[5,6] Satoru Takahashi,[4,6] Masazumi Nishimoto,[3] and Akihiko Okuda[1,4,*]
[1]Division of Developmental Biology
[2]Division of Functional Genomics and Systems Medicine
[3]Radioisotope Experimental Laboratory
Research Center for Genomic Medicine, Saitama Medical University, Yamane Hidaka, Saitama 350-1241, Japan
[4]Core Research for Evolutional Science and Technology (CREST)
[5]Precursory Research for Embryonic Science and Technology (PRESTO)
Japan Science and Technology Agency, Kawaguchi, Saitama 332-0012, Japan
[6]Department of Anatomy and Embryology, Institute of Basic Medical Sciences, Graduate School of Comprehensive Human Sciences, University of Tsukuba, 1-1-1 Tennodai, Tsukuba 305-8575, Japan
*Correspondence: akiokuda@saitama-med.ac.jp
DOI 10.1016/j.stem.2011.04.020

SUMMARY

Embryonic stem cells (ESCs) can self-renew indefinitely under the governance of ESC-specific transcriptional circuitries in which each transcriptional factor regulates distinct or overlapping sets of genes with other factors. c-Myc is a key player that is crucially involved in maintaining the undifferentiated state and the self-renewal of ESCs. However, the mechanism by which c-Myc helps preserve the ESC status is still poorly understood. Here we addressed this question by performing loss-of-function studies with the *Max* gene, which encodes the best-characterized partner protein for all Myc family proteins. Although Myc/Max complexes are widely regarded as crucial regulators of the ESC status, our data revealed that ESCs do not absolutely require these complexes in certain contexts and that this requirement is restricted to empirical ESC culture conditions without a MAPK inhibitor.

INTRODUCTION

ESCs are defined by their pluripotency and unlimited self-renewal (Nichols and Smith, 2009; Niwa, 2007; Rossant, 2008). These characteristics are sustained by numerous signal transduction pathways, including pathways that involve leukemia inhibitory factor (LIF) and bone morphogenic protein, and transcription factors including Oct3/4, Sox2, and Nanog (see Silva and Smith, 2008, and references therein). The transcription factor c-Myc is critically involved in maintaining the pluripotency and self-renewing properties of ESCs (Cartwright et al., 2005; Singh and Dalton, 2009). Accumulating evidence suggests that the function of c-Myc in ESCs is largely independent of the Oct3/4, Sox2, and Nanog networks (Hu et al., 2009; Kim et al., 2010).

Recent studies with *c-Myc/N-Myc* double-knockout (dKO) ESCs demonstrate that c-Myc and N-Myc, which have highly redundant functions, are required to maintain ESC self-renewal and pluripotency (Smith et al., 2010; Varlakhanova et al., 2010). Moreover, an examination of Myc molecular function in ESCs showed that the protein sustains pluripotency by repressing gene expression of the primitive endoderm master regulator *Gata6.* In addition, the Myc protein helps control the cell cycle by regulating the *mir-17-92* miRNA cluster (Smith et al., 2010). However, there are numerous unanswered questions about the roles of c-Myc in ESCs. For example, it is unknown whether there is a situation in ESCs in which Myc function may be redundant.

In this report, we demonstrate that ablating *Max* gene expression in ESCs, which encodes the best-characterized partner protein for c-Myc, N-Myc, and L-Myc proteins (Blackwood et al., 1992; Shen-Li et al., 2000), leads to a loss of the undifferentiated state and extensive cell death. Interestingly, these two phenomena occur in a compulsory order with the loss of the undifferentiated state occurring first, indicating that undifferentiated ESCs fail to execute the cell death program. More importantly, we provide evidence that the newly established ESC culture conditions by using MAPK and GSK3β inhibitors (Ying et al., 2008) render the c-Myc/Max complex dispensable. This indicates that ESCs are not necessarily dependent on the c-Myc/Max complex to preserve their prominent features and that this requirement is context dependent.

RESULTS

Myc/Max Complexes Are Required for ESC Self-Renewal and Cell Viability

To determine the molecular basis of the ESC-specific function of Myc, we generated *Max*-null ESCs in which both alleles of the *Max* gene are disrupted and *Max* cDNA was introduced into the *ROSA26* locus under the control of a tetracycline (tet)-off system (see Supplemental Experimental Procedures and Figures S1A–S1D; Masui et al., 2005). As depicted in Figure 1A, these *Max*-null ESCs did not express the *Max* gene in the presence of doxycycline (Dox), although the absence of Dox induced *Max* expression. We confirmed that both the *Max* mRNA and protein levels were rapidly downregulated by Dox addition to

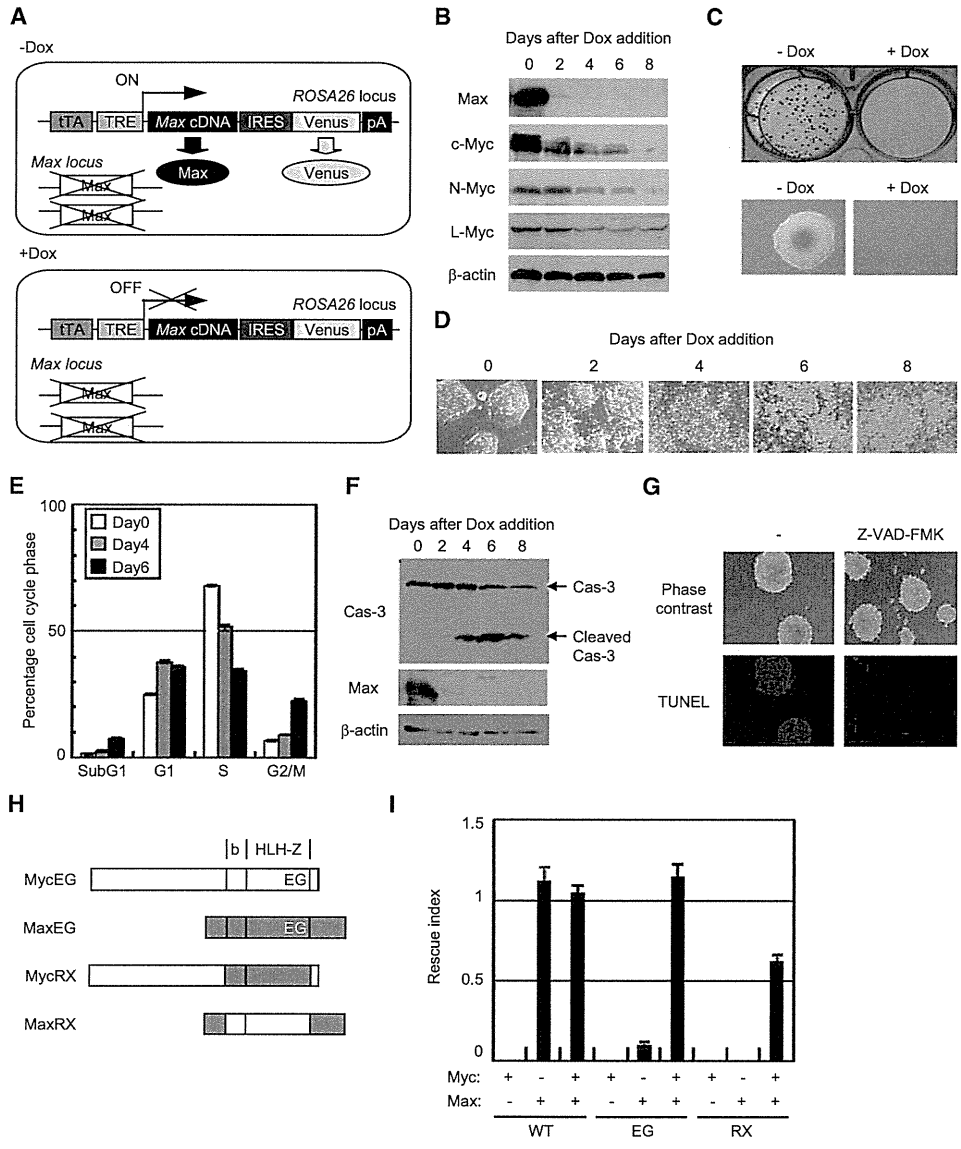

Figure 1. Myc/Max Complexes Have a Critical Role in ESC Viability

(A) Schematic representation of *Max*-null ESCs. *Max* and *Venus* from the *ROSA26* locus are expressed under the control of a tet-off system.

(B) Analyses of Max, c-Myc, N-Myc, and L-Myc protein levels after ablating *Max* expression.

(C) Viability examination of Dox-untreated and -treated *Max*-null ESCs. Viability was examined 12 days after seeding *Max*-null ESCs at a clonal density.

(D) Microscopy examination of ESCs after ablating *Max* expression.

(E) Cell cycle analysis of *Max*-null ESCs by FACS. The data represent the mean with standard deviation (n = 3).

(F) Detection of cleaved Cas-3 in *Max*-null ESCs.

(G) Effect of Z-VAD-FMK on *Max*-null ESC apoptosis. *Max*-null ESCs were either untreated or treated with Z-VAD-FMK for 6 days in the presence of Dox.

(H) Schematic representation of the EG and RX mutants of c-Myc and Max proteins. In the EG mutants, the amino acids in c-Myc and Max involved in their interaction are reciprocally exchanged (Amati et al., 1993).

(I) Rescue by c-Myc/Max mutant pairs. After stably introducing expression vectors encoding wild-type (WT) or the EG/RX mutants of c-Myc and/or Max, *Max*-null ESCs were treated with Dox for 6 days. The rescue index represents the relative number of colonies obtained in the absence of Dox. The data represent the mean with standard deviation (n = 3).

See also Figure S1.

the culture medium (Figures 1B and 3A). We also found that the protein levels of c-Myc, N-Myc, and L-Myc significantly decreased during the course of Dox-induced repression of Max protein expression (Figure 1B). This was consistent with a previous report that demonstrated free Myc proteins that are not associated with Max are more unstable than the proteins complexed with Max (Blackwood et al., 1992).

To examine the effect of ablation of *Max* gene expression on cell viability, *Max*-null ESCs were seeded at a clonal density, treated with Dox for 12 days, and then stained with Leishman's

stain. The Dox-treated cells did not form colonies, although the untreated cells formed robust colonies (Figure 1C). Moreover, microscopy examination of *Max*-null ESCs at various time points after Dox treatment revealed an abnormal morphology and severely impaired growth (Figure 1D). Cell cycle analyses indicated that ablation of *Max* gene expression led to a reduction in proliferation and cells with a sub-G1-phase that most probably reflected apoptosis (Figure 1E). Apoptotic cell death was also indicated by a TdT-mediated dUTP-biotin nick end-labeling (TUNEL) assay (Figure S1E) and the detection of cleaved activated caspase-3 (Cas-3) (Figure 1F). Treating with Z-VAD-FMK, a pan-caspase inhibitor, eliminated the appearance of TUNEL-positive cells (Figure 1G), indicating that caspase activation is responsible for the death of *Max*-null ESCs.

Max interacts not only with Myc family proteins but also with Mad family proteins that are natural Myc antagonists (Baudino and Cleveland, 2001). Moreover, some Mad family proteins, such as Mad3 and Mxi1, are highly expressed in ESCs (data not shown). Therefore, there is the possibility that functional inactivation of Mad family proteins, but not c-Myc family proteins, is the major cause of the lethal phenotype observed in *Max*-null ESCs. To examine this, we used the Max and Myc mutants depicted in Figure 1H, which were generated by Amati et al. (1993). These mutants were constructed either by exchanging the helix-loop-helix-leucine zipper (HLH-Z) domains (RX mutant) or reciprocally modifying the leucine zipper dimerization specificities (EG mutant; for details, see Amati et al., 1993). The RX mutants (also true for EG mutants) did not bind to their endogenous partners, but efficiently dimerized with each other. This was further confirmed by coimmunoprecipitation analyses (data not shown). We performed rescue experiments by stably transfecting *Max*-null ESCs with the expression plasmids. As expected, overexpressing wild-type Max alone led to efficient colony formation. For the EG and RX mutants, an equivalent level of efficiency was obtained only when a Max mutant (EG or RX) was introduced together with the reciprocal c-Myc mutant (Figure 1I). We observed weak activity when the Max EG mutant was expressed alone. We assumed that this activity indicated a partial preservation of the ability to interact with the wild-type c-Myc protein, as was previously reported (Amati et al., 1993). These results allowed us to conclude that the lack of functional Myc/Max complexes, but not Mad/Max complexes, is responsible for the detrimental phenotype of *Max*-null ESCs. It should be noted that, unlike loss of *Max* gene expression, simultaneous loss of *c-Myc* and *N-Myc* gene expression insignificantly impacted cell viability (Smith et al., 2010; Varlakhanova et al., 2010). Although we do not currently know why this happened, there are several possibilities that may explain these phenotypic differences (see Discussion).

A recent report with a chemical inhibitor (10058-F4) that disrupts the interaction between c-Myc and Max revealed that the complex augments gene expression by releasing RNA polymerase II (Pol II) around the gene promoter region rather than recruiting Pol II to the targeted gene (Rahl et al., 2010). Therefore, we examined whether Pol II is paused around the promoter-proximal gene regions in *Max*-null ESCs. This can be assessed by the positions of phosphorylation sites within the C-terminal domain (CTD) of the largest Pol II subunit. Although we confirmed the previously reported result by means of 10058-F4, no decline in the level of Pol II engaged in transcription elongation was evident in Dox-treated *Max*-null ESCs. This was indicated by the level of serine 2 phosphorylation in the CTD, which is directly proportional to the level of Pol II released from promoter proximal pausing (Figures S1F and S1G). We assumed that this discrepancy was due to the difference in rapidness of eliminating the interaction between c-Myc and Max. Approximately 2 days was required for complete Dox-mediated elimination of the Max protein and this may be long enough to execute a presently unknown alternative mechanism of Pol II release from gene promoters.

Alterations in Gene Expression after Ablating *Max* Gene Expression

Apoptosis observed with *c-Myc/N-Myc* dKO hematopoietic stem cells (HSCs) is mediated by upregulated *Grazyme B* gene expression (Laurenti et al., 2008). We examined expression of this gene and other related genes such as *Granzyme A* in *Max*-null ESCs. However, we found that these genes were not expressed in the cells, irrespective of treatment with Dox (data not shown). To explore the molecular basis of apoptosis and other phenotypes observed in *Max*-null ESCs, we performed DNA microarray analyses. First, we compared the gene expression between *Max*-null ESCs and *c-Myc/N-Myc* dKO HSCs. However, we did not find any obvious tendency that the genes regulated differentially in dKO HSCs compared with those in wild-type HSCs (Laurenti et al., 2008) altered their expression levels in a similar trend in *Max*-null ESCs (Figures S2A and S2B), indicating that gene sets regulated by Myc/Max complexes are rather different between ESCs and HSCs. As a next step, the genes with altered expression levels more than 2-fold (upregulated genes, 1696; downregulated genes, 1402) in *Max*-null ESCs were assigned to gene ontology (GO) classification to correlate gene expression changes with overall molecular functions. GO terms that were significantly enriched among the upregulated or downregulated genes are shown (Table S1). Among these GO terms, we were especially interested in a gene set associated with antioxidant activity because reactive oxygen species (ROS) can induce apoptosis and c-Myc is reported to suppress ROS levels (Benassi et al., 2006; Esteban et al., 2010). Gene set enrichment analysis (GSEA) (Subramanian et al., 2005) of genes comprising this GO term showed a prominent decrease in activity after ablation of *Max* gene expression, which was not seen in dKO HSCs (Figure S2C). To examine whether the reduction of antioxidant activity led to the alteration of the ROS level in *Max*-null ESCs, we quantitated the ROS in cells via DCF-DA fluorescence. Because *Max*-null ESCs cultured in the absence of Dox express Max and Venus fluorescence protein (see Figure 1A) that perturbs quantitation of the ROS level, we eliminated this expression from the *ROSA26* gene locus by treating with Dox, but we introduced the indicated expression vector(s) or empty vector randomly into the cell genome. As shown in Figure 2A, we found that a high ROS level was indeed detected in *Max*-null ESCs with the empty vector introduced, whereas the ROS level declined significantly with forced expression of Max. We did not observe an effect from coexpression of c-Myc and Max on the ROS level compared with Max expression alone, although we did observe a definite gene dosage effect when the cells were subjected to a more rigorous condition, i.e., culture without 2-mercaptoethanol (2-ME) (Figure 2B). These results suggested that the c-Myc/Max complex suppresses oxidative stress in

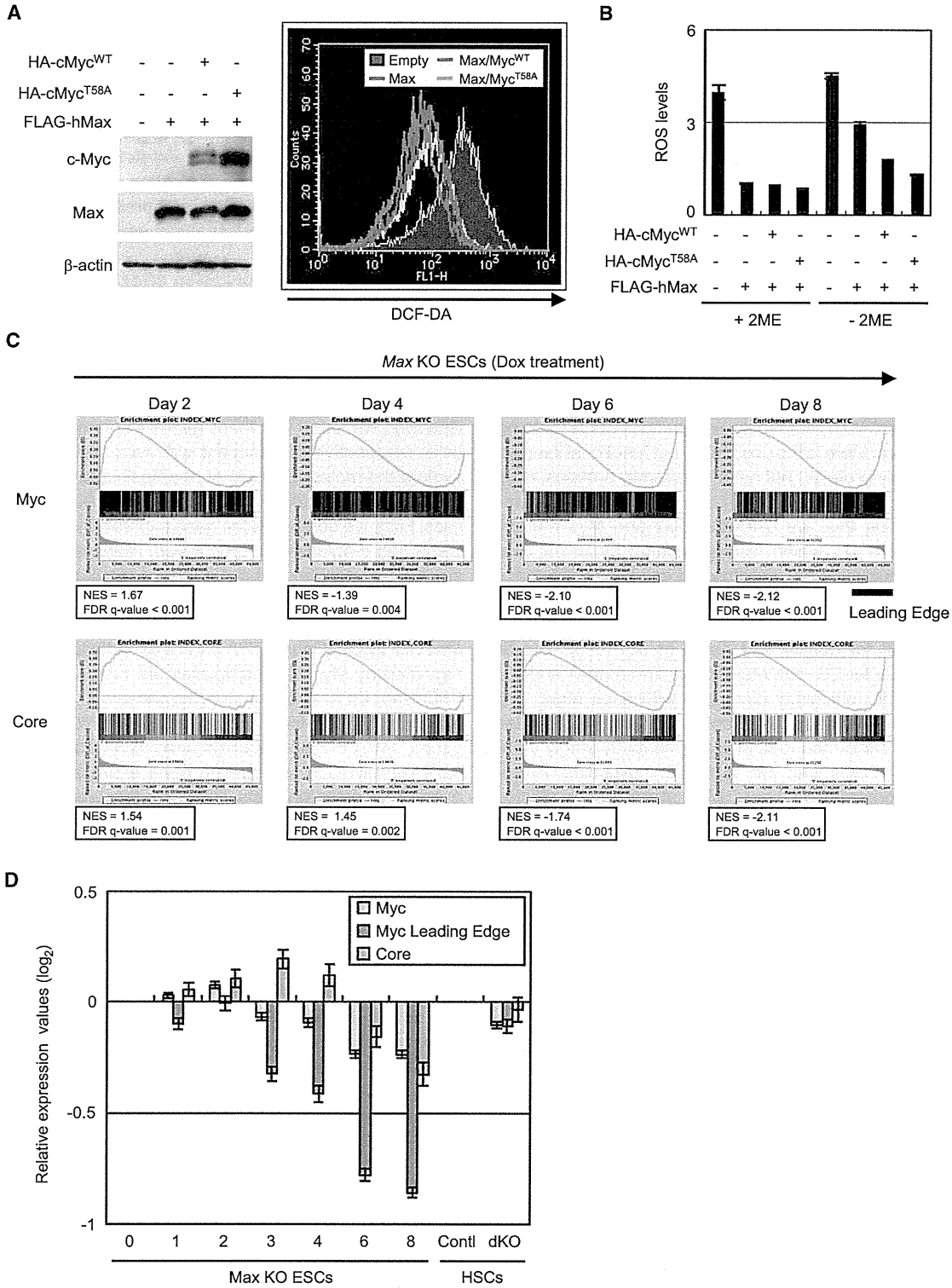

Figure 2. Alternation of ESC Gene Expression Programs after *Max* Gene Expression Ablation

(A) Quantification of intracellular ROS levels in *Max*-null ESCs transfected with the indicated expression plasmids via DCF-DA. Left panel shows Myc and Max proteins detected by western blot analysis. The cMyc^{T58A} is a stabilized c-Myc protein that evades GSK-3β-mediated phosphorylation that is coupled with proteolysis (Cartwright et al., 2005).

(B) Gene dosage effect of the c-Myc/Max complex on lowering the ROS level. *Max*-null ESCs transfected as in (A) were cultured in the presence or absence of 2-ME. Intracellular ROS levels were then quantitated with DCF-DA. The level of ROS observed with the cells in which Flag-tagged *Max* cDNA alone was introduced (lane 2) was arbitrarily set to one. The data represent the mean with standard deviation (n = 3).

ESCs and that apoptotic cell death observed with *Max*-null ESCs is at least in part due to the elevated ROS.

Recently, Wong et al. (2008) identified a predominant gene module with DNA microarray analyses, which was designated the ESC-like module that is commonly activated in ESCs as well as aggressive cancer cells. A recent report by Kim et al. (2010) also highlights the importance of analyzing transcriptional regulatory subnetworks in ESCs. This involves the gene expression signature of ESCs being dissected into three major functional modules (Core, Polycomb, and Myc). Of note, the Myc module is closely related to the core ESC-like module identified by Wong et al. (2008) but is distinct from the Core module that comprises genes regulated by core pluripotency factors such as Oct3/4 and Nanog. We monitored alterations of Myc and Core module activities by GSEA during loss of *Max* gene expression (Figure 2C). We found that the loss of *Max* gene expression led to a progressive decline in Myc module activities, although a slight increase was observed at day 2. We could also obtain similar results with the ESC-like module (Figures S2D and S2E). In contrast, we found the level of Core module activity was boosted for the first 4 days after ablating *Max* gene expression. However, at 6 days post-Dox addition, the level of Core module activity became negative compared with the Dox-untreated cells, implying that *Max*-null ESCs started to lose pluripotency. Although the decrease in Core module activity in *Max*-null ESCs was preceded by a reduction of Myc module activity, we do not know at present whether there is a functional link between these modules. As shown in Figure 2D, monitoring the changes in average expression levels of these modules after ablating *Max* gene expression gave rise to consistent results with GSEA shown in Figure 2C. We also calculated the average expression values of 206 genes representing the leading edge of the Myc module that are responsible for the decline in overall Myc module activity in *Max*-null ESCs at day 8 in GSEA (a list of individual gene names of this gene set is shown in Table S2). We found that these genes showed a more prominent decline after ablating *Max* gene expression compared with total Myc module genes (503 individual genes). GO analyses revealed that genes involved in nucleic acid and macromolecular metabolic processes and cellular process were remarkably enriched in Myc module leading edge genes (Table S3). Although the question remains whether or how these molecular functions are coupled to the phenotypes observed with *Max*-null ESCs, we could speculate that ESCs produce substantial amounts of energy due to these gene functions representing the metabolic processes to support their robust growth and self-renewing properties.

Depletion of *Max* Gene Expression Is Accompanied by Loss of the Undifferentiated State in ESCs through Activation of MAPK Signaling

We next investigated whether the undifferentiated state of ESCs was affected in the *Max*-null background. Semiquantitative RT-PCR analysis showed that there was no decline in the mRNA levels for pluripotency markers such as *Oct3/4* and *Nanog* upon loss of *Max* gene expression up to day 8 (Figure 3A). However, the total Core module activity assessed by DNA microarray analysis was eventually reduced in *Max*-null ESCs by day 6 (Figures 2C and 2D). This indicated that the overall activities of these key pluripotency factors decreased in these cells. Consistent with this assumption, western blotting revealed that the Oct3/4, Sox2, and Nanog protein levels gradually declined upon loss of *Max* gene expression (Figure 3B). Immunostaining (Figure 3C) and FACS analyses (Figure 3D) revealed that *Max*-null ESC colonies consisted of Oct3/4-positive and -negative populations. This suggested that the decline in Oct3/4 levels does not occur evenly, but occurs stochastically in the *Max*-null ESC population when examined within a very short period. Moreover, quantitative RT-PCR analysis of several lineage-specific markers demonstrated that loss of *Max* gene expression resulted in the upregulation of endoderm markers (*Gata6, Gata4*, and *Sox17*), ectoderm markers (*Fgf5, Sox1, Nestin*, and *Pax6*), and a trophectoderm marker (*Cdx2*), whereas mesoderm markers (*Brachyury* and *Desmin*) were not induced (Figure 3E). These results were not consistent with those obtained from *c-Myc/N-Myc* dKO ESCs with these cells selectively differentiating into primitive endoderm lineages (Smith et al., 2010). Currently, we do not know why these phenotypic differences occur. We also observed remarkably elevated levels of phosphorylated MAPK (ERK1/2) after Dox treatment (Figure 3F), which were inversely correlated with Oct3/4 protein levels. Because MAPK is known to destabilize the pluripotency of mouse ESCs (Buecker et al., 2010; Kunath et al., 2007; Niwa et al., 2009), we treated *Max*-null ESCs with PD0325901, a small molecule targeting MAPK kinase. This chemical treatment significantly blocked the decline of Oct3/4 and Sox2 and the emergence of Oct3/4-negative cells after depletion of *Max* gene expression (Figure 3G and 3H, also see Figure 4B). This implied that MAPK activation was the primary cause of cellular differentiation in *Max*-null ESCs. Also noteworthy is that PD0325901 treatment caused a tremendous decrease of the c-Myc protein level irrespective of Dox treatment, whereas the protein levels of other Myc members, i.e., N-Myc and L-Myc, and pluripotency markers such as Oct3/4, Sox2, and Nanog were not affected by PD0325901 alone (Figure 3G).

Hierarchical Relationship between the Loss of the Undifferentiated State and Apoptotic Cell Death in *Max*-Null ESCs

Although loss of *Max* gene expression elevated several differentiation markers, there were no surviving differentiated cells in the presence of Dox. This indicated that the detrimental phenotype persists in *Max*-null ESCs even after a differentiation program is initiated. Consistent with this notion, our data showed that

(C) GSEA of Myc and Core modules in *Max*-null ESCs at the indicated days after Dox administration with these modules in Dox-untreated *Max*-null ESCs as references. Black bar in the lower right of the Myc module panel at day 8 represents the leading edge genes of the Myc module.
(D) The fold changes in Myc module genes (yellow) and Core module genes (pink) are shown as the means with standard errors. The fold changes of expression levels of Myc module leading edge genes (orange), which were selected by GSEA shown in (C) as members responsible for the decline of overall Myc module activity, are also shown. Data obtained with the corresponding gene set at day 0 were used as references. The fold changes in these gene sets in *c-Myc/N-Myc* dKO HSCs compared with those in wild-type HSCs are also shown.
See also Figure S2 and Tables S1–S3.

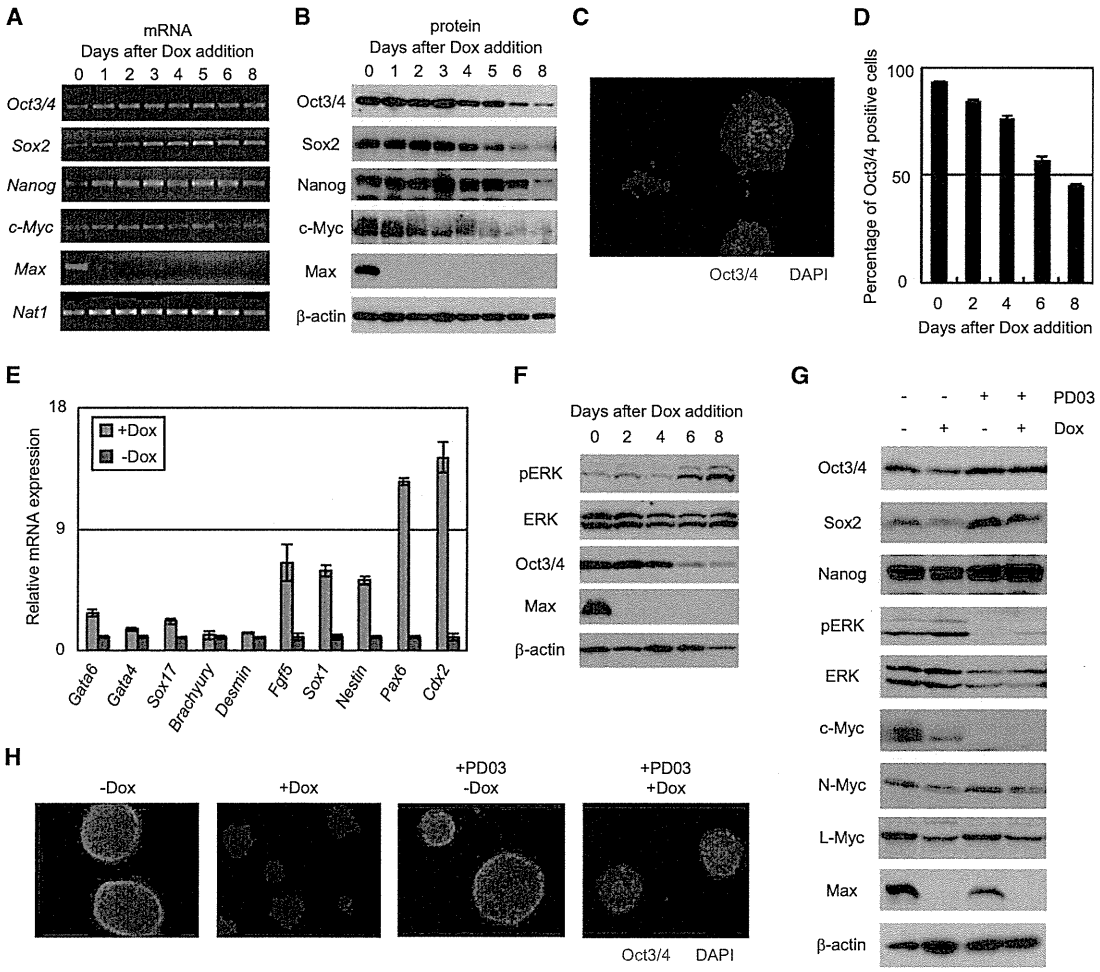

Figure 3. Gradual Loss of the Undifferentiated State of ESCs upon *Max* Expression Ablation

(A and B) Semiquantitative RT-PCR (A) and western blot analyses (B) of ESC markers, c-Myc, and Max in *Max*-null ESCs.

(C) Immunocytochemical analysis of Oct3/4 in *Max*-null ESCs treated with Dox for 6 days.

(D) FACS-based analysis of the Oct3/4-positive cell ratio upon the loss of *Max* expression. The data represent the mean with standard deviation (n = 3).

(E) Quantitative RT-PCR analysis of various cell-lineage marker genes with *Max*-null ESCs treated with Dox for 6 days. The data represent the mean with standard deviation (n = 3). The value obtained from Dox-untreated cells was arbitrarily set to one.

(F) Inverse proportion between Phospho (Thr202, Tyr204)-ERK and Oct3/4 levels after ablating *Max* expression.

(G) Effect of PD0325901 on ESC markers and Myc proteins in *Max*-null cells. *Max*-null ESCs were treated with PD0325901 (PD03) or untreated (–) in the presence or absence of Dox for 6 days.

(H) Effect of PD0325901 on the suppression of Oct3/4-negative cell emergence in *Max*-null ESCs. *Max*-null ESCs were treated as indicated for 6 days and then subjected to immunocytochemical analysis to detect Oct3/4.

Max-null ESCs did not form embryoid bodies (Figure S3A) or a teratoma (data not shown). These results promoted us to explore the relationship between the loss of the undifferentiated state and apoptotic cell death in *Max*-null ESCs. Coimmunocytochemical analysis showed that the presence of Oct3/4 and activated Cas-3 was mutually exclusive (Figure 4A). Z-VAD-FMK treatment suppressed the emergence of TUNEL-positive cells (Figure 1G) but not the conversion of Oct3/4-positive to -negative cells (Figure 4B). On the other hand, PD0325901 treatment prevented the emergence of Oct3/4-negative cells (Figure 4B) and eliminated TUNEL-positive cells (Figure S3B). These results indicate that loss of the undifferentiated state occurs first and is followed by the induction of apoptosis and that MAPK activation is substantially involved in loss of the undifferentiated state of *Max*-null ESCs. Western blot (Figure 4C) and FACS analyses (Figure 4D) that examined activated Cas-3 levels and pluripotency marker proteins supported this notion.

Forced *Nanog* Expression Renders *Max* Expression Redundant in ESCs

Thus far, our analyses revealed that c-Myc/Max complex loss of function in ESCs led to the loss of the undifferentiated state and a subsequent reduction in cell viability. Therefore, we hypothesized that *Max*-null ESCs can indefinitely self-renew if the undifferentiated state is maintained. To address this hypothesis, we first overexpressed Oct3/4. However, this provoked extensive

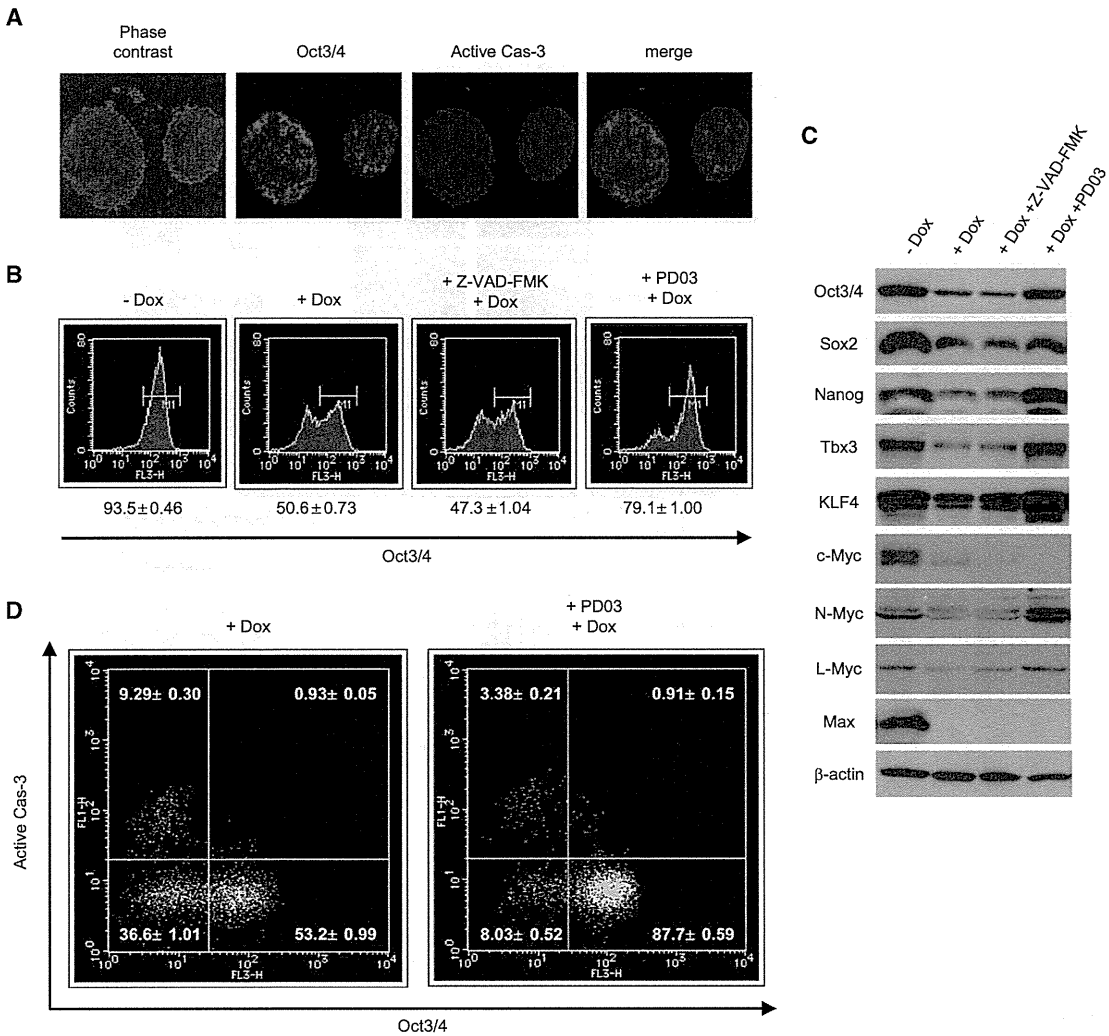

Figure 4. Compulsory Order between Loss of the Undifferentiated State and Apoptotic Cell Death in *Max*-Null ESCs

(A) Coimmunostaining of Oct3/4 and activated Cas-3 in *Max*-null ESCs treated with Dox for 6 days.

(B) Effects of Z-VAD-FMK or PD0325901 on the undifferentiated state. *Max*-null ESCs were treated as indicated for 6 days and then subjected to FACS analysis of Oct3/4 expression. The data represent the mean with standard deviation (n = 3).

(C) PD0325901, but not Z-VAD-FMK, was able to preserve normal levels of ESC marker proteins in *Max*-null ESCs. *Max*-null ESCs were untreated or treated with either Z-VAD-FMK or PD0325901 in the presence of Dox for 6 days. Dox-untreated *Max*-null ESCs were used as a control.

(D) Mutual exclusiveness of activated Cas-3 and Oct3/4 in *Max*-null ESCs and the effect of PD0325901 on their relative prevalence. Cells were treated with or without PD0325901 in the presence of Dox for 6 days and then subjected to FACS analysis. The data represent the mean with standard deviation (n = 3).

See also Figure S3.

differentiation (data not shown), consistent with a previous report demonstrating that expression level of Oct3/4 must be kept within plus or minus 50% of the endogenous expression level in order to maintain undifferentiated state of ESCs (Niwa et al., 2000). Then, we overexpressed *Klf4*, *Tbx3*, and *Nanog*, which allow ESCs to self-renew independently of LIF (Niwa et al., 2009). Although *Klf4* and *Tbx3* expression did not affect *Max*-null ESCs, forced *Nanog* expression prevented the decline in Oct3/4 and Sox2 protein levels (Figure 5A) and produced viable colonies (Figure 5B). The *Nanog*-expressing *Max*-null ESCs were able to expand continuously even in the presence of Dox for at least 3 months without any change in colony morphology. These rescued cells were homogeneously positive for Oct3/4 and Nanog (Figure 5C) and were TUNEL negative (Figure S4A). Consistent results were obtained from western blot analysis that examined the expression levels of pluripotency marker proteins and activated Cas-3 (Figure 5D). Interestingly, expression levels of c-Myc, N-Myc, and L-Myc in *Nanog*-rescued cells was comparable to those in Dox-untreated cells, suggesting that Nanog stabilizes Myc proteins free from Max through a presently unknown mechanism. Cell proliferation rate (Figure 5E) and cell cycle (Figure 5F) analyses indicated that the defects observed with Dox-treated cells were completely eliminated by forced *Nanog* expression. Collectively, these results indicated that forced *Nanog* expression renders *Max* expression dispensable for the unlimited self-renewal of ESCs. We also examined

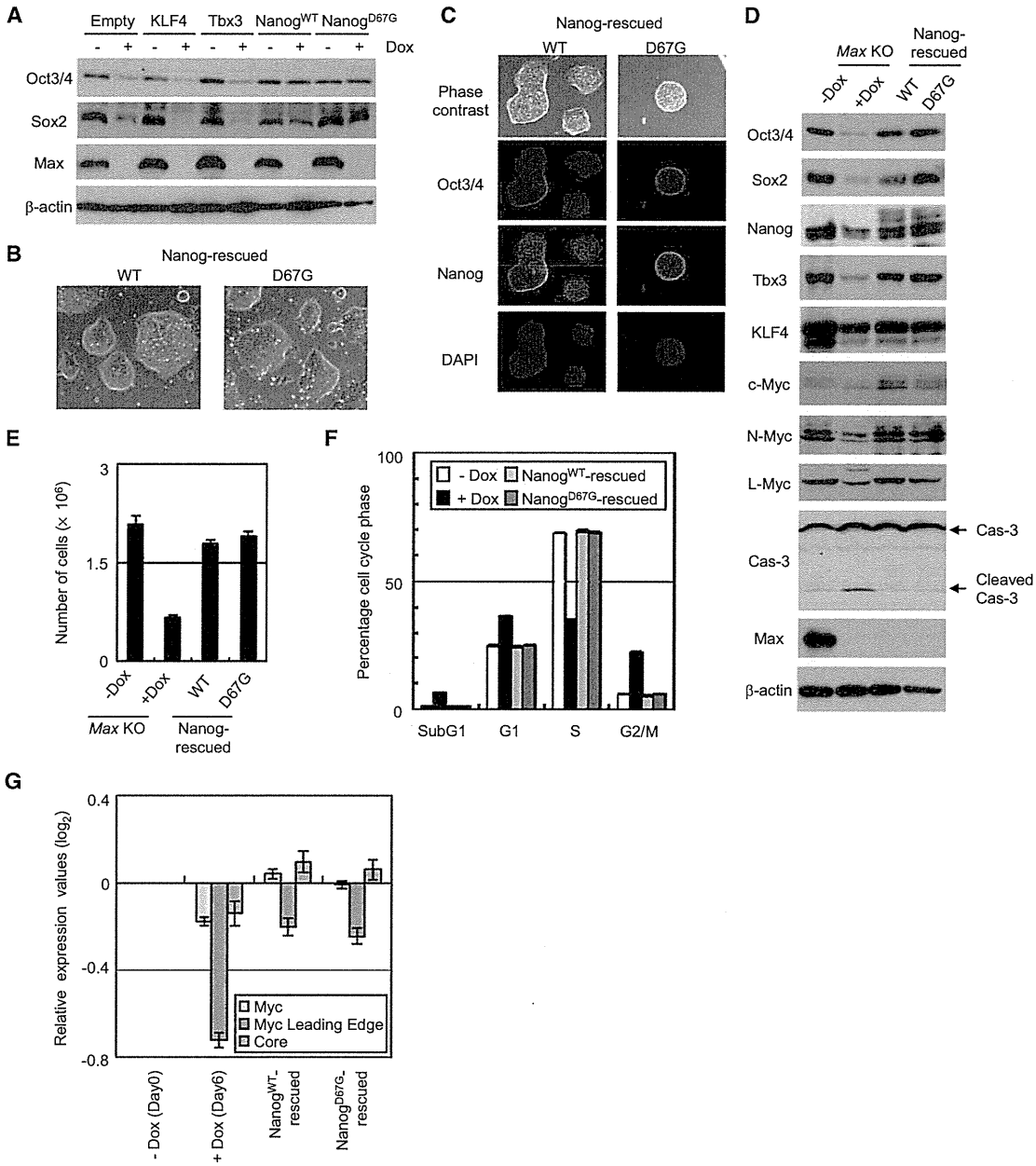

Figure 5. Forced *Nanog* Expression Results in the Long-Term Preservation of ESC Self-Renewal in the Absence of *Max* Expression

(A) *Max*-null ESCs were stably transfected with expression vectors encoding KLF4, Tbx3, wild-type (WT), or a caspase-resistant mutant (D67G) of Nanog. After Dox treatment for 6 days, cell lysates were prepared and subjected to western blot analysis with the indicated antibodies.

(B) Microscopy inspection of *Nanog*-rescued cells.

(C) Immunocytochemical analysis of Oct3/4 and Nanog in *Nanog*-rescued cells.

(D) Western blot analysis of ESC markers, Myc family proteins, and activated Cas-3 in *Nanog*-rescued cells.

(E) The proliferation rate of *Nanog*-rescued cells. Ten thousand respective stable cells were plated and the total cell number was counted 4 days after treating with Dox. The data represent the mean with standard deviation (n = 3).

(F) Cell cycle analysis of *Nanog*-rescued cells by FACS. The data represent the mean with standard deviation (n = 3).

(G) Myc and Core module activities in *Nanog*-rescued *Max*-null ESCs. Data were obtained as in Figure 2B.

See also Figure S4.

the ability of a modified form of Nanog, D67G, which is resistant to caspase-mediated cleavage (Fujita et al., 2008), to impact the self-renewal of ESCs. However, we did not detect any differences between wild-type Nanog and the D67G mutant to counteract the loss of pluripotency and impaired cell viability (Figures 5B–5F). This finding reinforced the notion that there is a hierarchical order in the loss of the undifferentiated state and cell viability in *Max*-null ESCs in which the caspase-dependent

apoptosis pathway is initiated only after loss of the undifferentiated state. We examined whether expression of RNA polymerase III (Pol III) target genes was normal or affected in *Max*-null ESCs and Nanog-rescued cells, because Myc is known to support transcription of these genes independently of Max (Gomez-Roman et al., 2003; Steiger et al., 2008). RT-PCR analysis revealed that both Nanog-rescued and Dox-treated *Max*-null ESCs, which maintain normal and reduced levels of Myc proteins, respectively, supported normal levels of expression for all Pol III target genes examined (Figures S4B and S4C). These results implied that a low Myc protein level in Dox-treated cells was enough to support Pol III target gene expression. Alternatively, certain compensatory mechanisms may have been operative in these cells.

We next examined how forced *Nanog* expression affects the level of Myc and Core module activities in the rescued *Max*-null ESCs (Figure 5G). As shown in Figure 2D, both module activities in *Max*-null ESCs were significantly impaired by Dox treatment for more than 6 days. However, we found that no decline in Core module activity became evident in Nanog-rescued cells. Unexpectedly, *Max*-null ESCs also regained Myc module activity to a normal level with forced *Nanog* expression. However, the average expression values of genes comprising the leading edge of the module remained below that of Dox-untreated *Max*-null ESCs. This implied that Nanog did not fully engage in restoring the Myc module program to the original state as observed with Dox-untreated *Max*-null ESCs. However, Nanog did somehow boost the average module activity through a distinct pathway from that of Myc/Max complexes.

The 2i Condition Renders Myc/Max Complexes Dispensable in ESCs

We found that PD0325901 counteracted the strong negative effect of *Max* gene expression ablation on the preservation of the undifferentiated state and cell viability (see Figure 4B and Figure S3B as references). However, the rescue effect of PD0325901 was not complete and loss of the undifferentiated state and cell death became prominent after several passages (data not shown). Recently reported is that *c-Myc* gene expression levels are unusually low when ESCs are exposed to a so-called ground state or related condition via PD0325901 and CHIR99021, a specific GSK-3β inhibitor, i.e., the 2i condition (Ying et al., 2008). Therefore, we hypothesized that the 2i condition preserves the ESC status without using Myc/Max transcriptional complexes. To test this hypothesis, we cultured *Max*-null ESCs with PD0325901 and CHIR99021 in the presence of Dox. We found that the 2i condition almost completely rescued *Max*-null ESCs (Figure 6A) and the colonies could be passaged at least 30 times with no change in morphology compared with *Max*-null ESCs that were not Dox treated, although the 2i-rescued cells did have a slightly slower proliferation rate. We next added a sirt1 inhibitor, nicotinamide (Nam) (Chong et al., 2005), while the cells were being treated with the 2i condition because our data revealed that sirt1 is substantially involved in *Max*-null ESC apoptosis (T.H. and A.O., unpublished data). We found that the 2i/Nam condition rendered Dox-treated *Max*-null ESCs completely indistinguishable from untreated cells, even with respect to the proliferation rate. Figure 6B shows the homogeneous expression of Oct3/4 and Nanog in cells that were rescued with 2i or 2i/Nam. Western blot analysis (Figure S5A) revealed that the expression levels of pluripotency markers, including Tbx3 and Klf4, in the rescued cells were comparable with control Dox-untreated *Max*-null ESCs. The activated Cas-3 level in *Max*-null ESCs also concomitantly declined because of the 2i and 2i/Nam treatments.

To rule out the possibility that the rescue effect of the 2i treatment depended on "leaky" *Max* gene expression from the *ROSA26* locus, which can be detected even with Dox, we generated three independent ESC clones (clone 31, 32, and 35) in which a Dox-regulatable *Max* expression unit is removed from the locus, while the cells were exposed to 2i condition (see Figure S5B for strategy). Lack of Max protein and of the gene expression were confirmed by western blot (Figure 6C) and Southern blot (Figure S5B) analyses, respectively. These strictly *Max*-null ESCs could be expanded while maintaining their ESC status (see Figure S5C and Figure 6C for their viability and Oct3/4 expression, respectively). However, these cells underwent extensive cell death irrespective of Dox absence when transferred to empirical culture conditions for mouse ESCs (Figure S5C). Thus, these results further reinforced the context-dependent requirement of Myc/Max complexes to preserve the undifferentiated state of ESCs.

To test whether the 2i/Nam-rescued cells could re-enter embryonic development once *Max* expression was regained, *Max*-null ESCs bearing Dox-regulatable *Max* cDNA and the strictly *Max*-null clone 31 were labeled with fluorescent Kusabira-Orange protein under the 2i/Nam condition. Subsequently, these cells were subjected to mouse chimera analysis. Although we observed a minor contribution from the strictly *Max*-null cells in one out of six 6.5 d.p.c. embryos (Figure S5D and Table S4), these cells failed to contribute to embryos at later stages (Figure 6D and Table S4). These results were consistent with the embryonic lethal phenotype of the *Max* knockout mouse at ~E6.5 (Shen-Li et al., 2000). However, *Max*-null ESCs carrying Dox-regulatable *Max* cDNA contributed to the entire epiblast portion of 6.5 d.p.c. embryos (Figure S5D) and to all three germ layers of 9.5 d.p.c. embryos (Figure 6D), although these levels of contribution from the embryo-injected cells progressively declined after E10.5 (see Table S4). These results indicate that *Max*-null ESCs maintained in the 2i/Nam plus Dox condition at least preserve all of requirements to differentiate into derivatives of all three germ layers during mouse development except the Max protein. However, our data also indicate that these cells are not completely equivalent to wild-type ESCs and show some defect in their pluripotency even if *Max* expression is complemented.

Next, we investigated the effect of *Max* gene expression ablation on gene expression profiles of ESCs cultured under 2i/Nam condition. We found that a substantial number of genes showed significant differences in their expression levels between wild-type and strictly *Max*-null ESCs cultured under 2i/Nam conditions, although the variable levels were significantly less prominent compared to the case with a conventional culture condition (Figure S6A). Alteration of gene expression between these two cell populations under 2i/Nam condition was also shown with a heat map (Figure S6B). We assume that some of the genes identified in these analyses may be responsible for some defect of 2i/Nam-rescued *Max*-null ESCs in their pluripotency, which

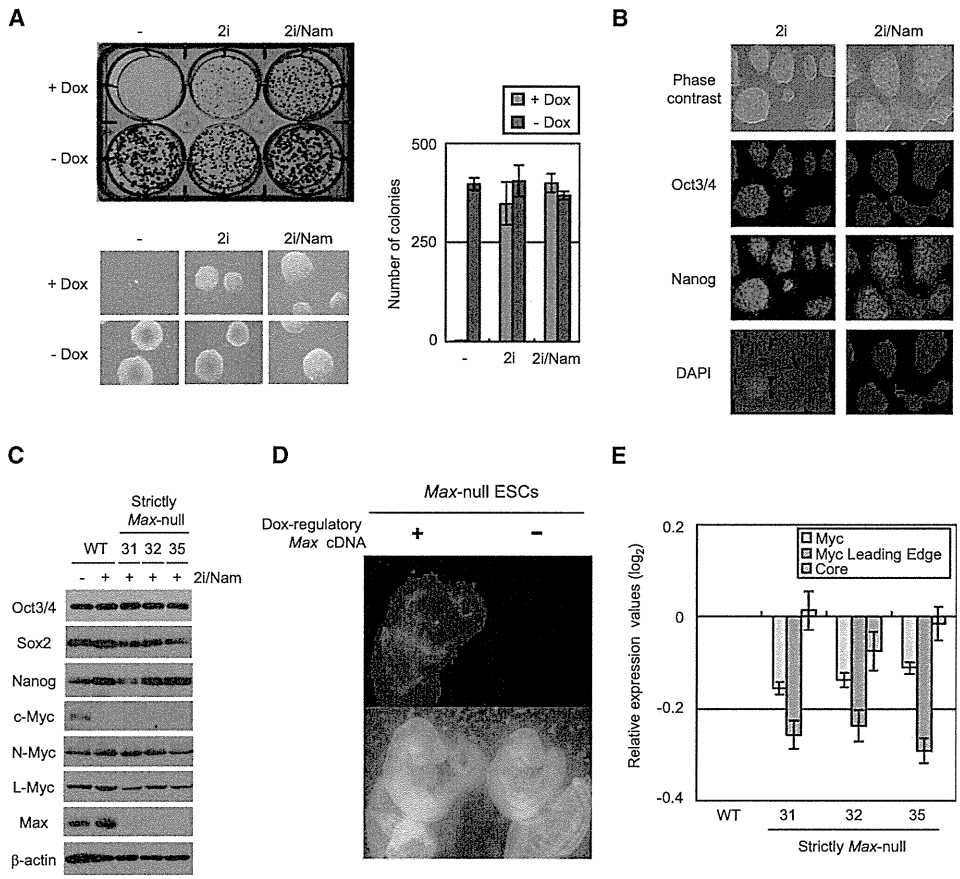

Figure 6. The 2i Condition Preserves the ESC Status through a Myc/Max Complex-Independent Mechanism

(A) Treating with 2i or 2i/Nam erased the lethal phenotype of *Max*-null ESCs. Cell viability was examined as in Figure 1C with *Max*-null ESCs treated with 2i or 2i/Nam.

(B) Immunostaining analysis of Oct3/4 and Nanog in 2i- and 2i/Nam-rescued cells.

(C) Western blot analysis of ESC markers and Myc family proteins in wild-type and strictly *Max*-null ESCs with the Dox-regulatable *Max* expression unit in the *ROSA26* gene locus removed under 2i/Nam conditions.

(D) Chimeric mouse analysis. Fluorescent Kusabira-Orange protein-labeled *Max*-null ESCs with or without a Dox-regulatable *Max* expression unit were injected into blastocysts. Embryos were allowed to develop in recipient female mice. Fluorescent and bright-field images of embryos recovered at E9.5 are shown. The rescued *Max*-null ESCs with 2i produced equivalent results (see Table S4).

(E) Myc and Core module activities in wild-type and strictly *Max*-null ESCs cultured under the 2i/Nam condition. The fold change of each gene set was calculated and shown as the means with standard errors. Data obtained with the corresponding gene set of the wild-type ESCs (WT) cultured under 2i/Nam condition were used as references.

See also Figures S5 and S6 and Table S4.

became evident with chimeric mouse analyses (Figure 6D and Table S4). Because two of Myc module members were included in the gene list which declined their expression more than 4-fold (Figure S6B), we next examined the Myc module activity. This analysis revealed that the module activity was significantly declined in strictly *Max*-null ESCs compared to that of wild-type ESCs even under the 2i/Nam condition (Figure 6E). Since *c-Myc* expression was barely detectable in the 2i/Nam condition (see Figure 6C), other Myc protein members, i.e., N-Myc and L-Myc, may contribute to Myc module activity in wild-type ESCs for this condition. More importantly, strictly *Max*-null ESC lines had Core module activity comparable with that of wild-type ESCs (Figure 6E). Data from GSEA supported this notion (Figure S6C). Thus, these data indicated that, unlike ESCs cultured under a conventional culture condition, decline of Myc module activity does not couple to the impairment of Core module activity and, therefore, provide additional evidence that the 2i condition can preserve the ESC status independently of Myc/Max transcriptional complexes.

DISCUSSION

Accumulating evidence has placed c-Myc at the heart of the regulatory network that governs the undifferentiated state of ESCs (Cartwright et al., 2005; Hu et al., 2009; Singh and Dalton, 2009; Smith et al., 2010; Varlakhanova et al., 2010). Recently discovered was that c-Myc regulates the *mir-17-92* miRNA to create the typical ESC cycle profile and represses *Gata6* expression to prevent cellular differentiation. However, numerous key questions remain unanswered. For example, it was not known